



34 have a smaller role in cluster formation but contribute to the consecutive growth process. According to
35 ion cluster measurements and kinetic model results, dimethylamine is not sufficient to stabilize all of
36 the sulfuric acid during springtime in the Po Valley, suggesting that other amines and ammonia can also
37 be involved. Generally, the high formation rates of sub-2 nm particles ($87 \text{ cm}^{-3} \text{ s}^{-1}$) and nucleation mode
38 growth rates (5.1 nm h^{-1}) together with the relatively low condensational sink ($8.9 \times 10^{-3} \text{ s}^{-1}$) will result
39 in a high survival probability of newly formed particles, making NPF crucial for the springtime aerosol
40 number budget in the Po Valley region.

41 **1. Introduction**

42 New particle formation (NPF) occurs ubiquitously in the troposphere and affects the global climate
43 (Dunne et al., 2016) and local or regional air quality (Kulmala et al., 2021). NPF and further growth of
44 the newly formed particles dominate aerosol number concentrations and are the major contributor to
45 the ultrafine ($<100 \text{ nm}$) aerosol budget, which poses a significant health threat to the population in
46 polluted areas (Schraufnagel, 2020). While air pollution mitigation strategies mostly focus on reducing
47 particulate mass (particulate matter below $2.5 \mu\text{m}$ ($\text{PM}_{2.5}$)), ultrafine particle number concentrations
48 might not be affected by such policies (De Jesus et al., 2019). It is therefore essential that we understand
49 the mechanisms leading to NPF in polluted environments to design better targeted air quality strategies
50 for polluted European regions, where $\text{PM}_{2.5}$ reduction measures are already implemented.

51 In theoretical calculations, it is generally assumed that NPF events are more favorable to occur in clean
52 conditions due to lower concentrations of preexisting aerosols, which act as condensational sink (CS),
53 capable of scavenging the gaseous precursors (Kulmala et al., 2017). However, frequent NPF events
54 have also been observed in heavily polluted urban environments (Kulmala et al., 2017; Du et al., 2022),
55 including megacities in China (Chu et al., 2019; Yao et al., 2018) and India (Sebastian et al., 2022).
56 This phenomenon might be associated with the overestimations of CS (Du et al., 2022) and the
57 involvement of multiple precursors in the complex polluted environment (Cai et al., 2023b). Various
58 studies have reported NPF precursors in strongly anthropogenically impacted environments. For
59 instance, in Shanghai and Beijing, China, sulfuric acid (SA, H_2SO_4) and amines were identified as key
60 contributors (Yao et al., 2018; Cai et al., 2021; Yan et al., 2021). In Barcelona, Spain, NPF was reported
61 to be associated with SA along with highly oxygenated organic molecules (HOMs) (Brean et al., 2020).
62 Meanwhile, some studies also address the importance of photooxidation products of vehicle emitted
63 organic vapors to NPF in Chinese megacities (Guo et al., 2020). Generally, NPF in the polluted regions
64 exhibits comparable growth rates and higher formation rates (J) compared to clean environment,
65 making it the dominant contributor to the number concentration of $\text{PM}_{2.5}$ in urban environment
66 (Kulmala et al., 2021).

67 The Po Valley region is one of the most important industrial and agricultural areas in Southern Europe
68 with dense population ($>17 \text{ million}/70,000 \text{ km}^2$). It is located in northern Italy, surrounded by the Alps
69 (in the north), the Apennine mountains (in the south), and the Adriatic Sea (in the east). High primary
70 anthropogenic emissions, a mixture of numerous pollutants from industrial, urban and agricultural
71 sources, together with frequently occurring stagnant meteorological conditions in winter make the Po
72 Valley region a hotspot in Europe for high aerosol loadings (Saarikoski et al., 2012; Li et al., 2014;
73 Finzi and Tebaldi, 1982; Daellenbach et al., 2023). At the same time, NPF occurs frequently in the Po
74 Valley (Hamed et al., 2007; Manninen et al., 2010). For example, Shen et al. (2021) observed that NPF
75 events took place on approximately 70% of the days during spring and summer. Similarly, Kontkanen
76 et al. (2017) discovered that during summer, NPF occurred on 89% of the days. During NPF event days,
77 high formation rates of sub-2nm neutral particles (J_2 , $\sim 10^1$ to $10^2 \text{ cm}^{-3} \text{ s}^{-1}$, (Kontkanen et al., 2017)) and
78 SA concentrations ($\sim 1 \times 10^7 \text{ cm}^{-3}$) were observed in the Po Valley (Paasonen et al., 2010; Kontkanen et
79 al., 2017). These levels were among the highest recorded in a study conducted at nine sites across the
80 Northern Hemisphere (Kontkanen et al., 2017).



81 The aforementioned studies mainly characterized the NPF process in the Po Valley based on particle
82 size distribution observations in terms of NPF frequency, nucleation and growth rates. Detailed
83 knowledge on the mechanisms of NPF and further growth in the Po Valley is still limited. In this study,
84 with a 2-month field campaign in the months of March – April 2022, we 1) identified the chemical
85 composition of atmospheric neutral and ion clusters by a set of state-of-the-art mass spectrometers, 2)
86 characterized the initial NPF and further growth rates using particle number size distribution
87 measurement down to 1 nm, and 3) compared the field measurement results with the recent Cosmics
88 Leaving Outdoor Droplets (CLOUD) chamber experiments to investigate the mechanism of NPF events
89 in the Po Valley region. This allowed us to elucidate the NPF and growth mechanisms at a severely
90 polluted Southern European site, and to give insights in best mitigation strategies for ultrafine particle
91 pollution in the context of already implemented PM_{2.5} reduction strategies.

92 **2. Method**

93 **2.1 Measurement site**

94 Our measurement was part of the Fog and Aerosol InterRAction Research Italy (FAIRARI) field
95 campaign in San Pietro Capofiume (SPC, 44.65°N, 11.62°E, 5 m a.s.l.), located in the Po Valley region
96 in Northern Italy. The measurement site is part of the Aerosol, Clouds and Trace Gases Research
97 Infrastructure (ACTRIS)-Italy network and operated by the Italian National Research Council-Institute
98 of Atmospheric Sciences and Climate (CNR-ISAC). The SPC site is approximately 30 km northeast of
99 Bologna (~400, 000 residents) and 20 km south of Ferrara (~130, 000 residents), the two major cities
100 in the area. The distance from the measurement site to the Adriatic Sea (to the east) is about 50 km. The
101 area around the sampling site consists of agricultural fields and a smaller town (<2, 000 inhabitants,
102 within 5 km) and smaller settlements in the proximity. Given its location, the SPC rural station is
103 considered to be representative of the regional background of the Po Valley (Paglione et al., 2021;
104 Paasonen et al., 2010; Hamed et al., 2007; Saarikoski et al., 2012; Decesari et al., 2014; Paglione et al.,
105 2020). The instruments for the NPF measurement were operated in a temperature controlled (~20 °C)
106 container from March 1 to April 30, 2022.

107 During the sampling period, the daily average temperature ranged from 1°C to 17°C. The average wind
108 speed (WS) was approximately 2.4±1.5 m/s (Fig. 1b). The average WS in the daytime was 3.5 m/s from
109 the east, which was significantly higher than at night (1.5 m/s) from the west. Strong diurnal variations
110 of wind direction were observed, which was typically from the west at night and shifted to the east
111 during the day (Fig. 1a). This pattern was potentially influenced by the sea-land breeze from the Adriatic
112 Sea. Accordingly, the daily average relative humidity (RH) varied from 41% to 98%, with values as
113 high as 85% at night, which sharply decreased to around 40% at noon caused by the strong temperature
114 variation.

115 **2.2 Instruments**

116 **2.2.1 Chemical composition measurements**

117 The chemical composition of cluster ions was measured using a high-resolution atmospheric-pressure-
118 interface time-of-flight mass spectrometer (APi-TOF, Aerodyne Research Inc. & ToFwerk AG). The
119 APi-TOF measures naturally charged ions present in the ambient environment. A detailed description
120 of the instrument can be found in Junninen et al. (2010). In this study, ambient air was sampled through
121 a 0.57-meter stainless steel tube with a flow rate of ~10 liters per minute (LPM), with 0.8 LPM of the
122 sample flow entering the APi-TOF.

123 The concentration of SA was measured using a nitrate ion (NO₃⁻)-based chemical-ionization (CI)
124 atmospheric-pressure-interface time-of-flight mass spectrometer (CI-APi-TOF, Aerodyne Research Inc.
125 & ToFwerk AG (Jokinen et al., 2012)). The CI-APi-TOF is an APi-TOF coupled with a CI-unit,
126 equipped with a soft X-ray source (L9490, Hamamatsu's 9.5 kV) to produce the primary ions. The
127 sampling flow went into the instrument through a ~0.6-meter ¾ inch stainless steel tube. The sampling
128 flow was 10 LPM and the sheath flow was set to 20 LPM. Data acquisitions for CI-APi-TOF was



129 performed with a time resolution of 10 s. A calibration factor of $1.0 \times 10^{10} \text{ cm}^{-3}$ for SA was determined
130 with sampling loss corrections before the campaign according to the method proposed by Kurten et al.
131 (2012).

132 Dimethylamine (DMA) measurements were performed using a Vocus CI-ToF (time-of-flight) mass
133 spectrometer (hereafter Vocus, Aerodyne Research Inc. & ToFwerk AG) using H_3O^+ as a reagent ion.
134 The Vocus has been described in detail in Krechmer et al. (2018) and the study by Wang et al. (2020)
135 utilized Vocus for DMA observations. In this study, the Focusing Ion-Molecular Reactor (FIMR) of
136 Vocus operated at a pressure of 2.0 mbar and a temperature of 100 °C with the radio frequency
137 amplitude of 350 V and frequency of 1.4×10^6 Hz. Data acquisition was performed with a time
138 resolution of 10 s in the mass range 0–1000 amu.

139 2.2.2 Particle size distribution measurements

140 Particle Size Magnifier

141 The Airmodus A11 nano-CNC-system (nano-Condensation Nucleus Counter), colloquially known as
142 the Particle Size Magnifier (PSM) is a two-step condensation particle counter (CPC) capable of
143 measuring particle size distributions of sub-3nm particles (Vanhanen et al., 2011). The system consists
144 of two parts, in which the PSM (Airmodus A10) acts as a preconditioner where particles are grown first
145 before being funneled to the CPC (Airmodus A20) for further growth and optical detection. In the PSM
146 the sample flow is turbulently mixed with a heated flow saturated with diethylene glycol (DEG) in the
147 mixing section and the DEG then condenses on the particles in the growth tube. By scanning the flow
148 rate through the DEG saturator, the smallest activated particle size is altered which can be converted
149 into a sub-3nm particle size distribution. Further particle growth is achieved by butanol in the CPC such
150 that the particles reach optically detectable sizes.

151 The PSM was calibrated according to the standard operation procedure for PSM (Lehtipalo et al., 2022)
152 using a known aerosol population from a glowing tungsten wire generator. The detection efficiency for
153 different particle sizes was determined by comparing the concentration of size selected particles to a
154 reference instrument, in this case a Faraday cup electrometer (FEC).

155 The system was set up with an Airmodus Nanoparticle Diluter (AND) inlet (Lampimäki et al., 2023)
156 for sample dilution and automatic background measurement to make sure that the CPC stays within a
157 single counting range during the campaign. The inlet was set up at around 2 meters above the ground
158 and the background was measured roughly every 8 hours and subtracted from the signal during the
159 inversion process.

160 HFDMPs and DMPS

161 The high-flow differential mobility particle sizer (HFDMPs) system utilizes a half-mini differential
162 mobility analyzer (DMA) to size-select particles that are then grown and detected by an A11 nano
163 Condensation Nucleus Counter system (Airmodus Ltd., A11 nano-CNC) (Kangasluoma et al., 2018).
164 The HFDMPs significantly improves sub-10 nm particle measurements compared to a typical
165 differential mobility particle sizer (DMPS) system, allowing us to better characterize the sub-10 nm
166 particle size distribution when combined with the PSM measurements. The A11 nano-CNC system was
167 size-calibrated with electro sprayed positively charged monomer ions of tetraheptylammonium bromide
168 (THA⁺) (Ude and De La Mora, 2005).

169 The HFDMPs inlet was set up at a height of 1 m and used a 50 cm long 10 mm outer diameter tube
170 with a core sampling system to minimize losses. A home-built Soft X-Ray ionization source (similar to
171 the TSI Inc. Model 3087) was used to charge particles. The HFDMPs measured the particle size-
172 distribution from 2–15 nm for both polarities at 15 predefined size-steps within 10 minutes (Fernández
173 De La Mora and Kozlowski, 2013).



174 Sampling from the same inlet and using the same charging device, a conventional DMPS system
175 equipped with a Hauke-type DMA (aerosol flow 1 LPM, sheath flow 5 LPM) and a TSI Inc. CPC
176 (Model 3772) was measuring the particle size-distribution from 10–800 nm at 16 predefined size-steps
177 within 10 minutes. In addition, a DMPS measuring from 15–800 nm was available in another
178 measurement container at the same field site. The total particle number concentrations measured
179 routinely with the CPCs after a size-scanning cycle of each DMPS system was compared with a
180 reference CPC (TSI Inc. Model 3025A) operated at the same site during the first weeks of the campaign.
181 It revealed on average a factor of 2 lower concentrations measured by the Hauke-type DMPS which
182 was confirmed to be rather size-independent by a comparison of the measured size-distributions and
183 their overlap with the Halfmini-DMPS system and was thus subsequently corrected for.

184 **2.2.3 Co-located measurements**

185 Additional co-located measurements of auxiliary data from CNR-ISAC network (www.isac.cnr.it/en)
186 and from the routine monitoring program of the Regional environmental protection agency of Emilia
187 Romagna (ARPAE, <https://www.arpae.it/it>) were used in this study. Trace gases were also measured
188 with 1 minute time resolution: O₃ (Thermo Scientific, model TEI-49i), NO_x (Teledyne-API, model
189 200A), NH₃ (Teledyne-API, model 201E), and SO₂ (Thermo Scientific, Model 43i Trace Level-
190 Enhanced). Moreover, meteorological parameters (e.g., RH, temperature, wind direction and wind
191 speed) were measured by a meteorology station (VAISALA Ltd, model wxt536).

192

193 **2.3 Data processing**

194 **2.3.1 New particle formation classification**

195 We classified each day according to whether a growing mode appeared in the particle size distribution
196 or not. This classification was done separately for both the DMPS and the PSM size distributions. A
197 growing mode was defined as a new particle mode that appeared in the particle size distribution and
198 continued to grow to larger sizes for at least two hours. If there was a growing mode visible in both the
199 PSM and DMPS size distributions, the day was defined as "NPF with growth". If there was no growth
200 or the growth was unclear in the DMPS size distribution but there was a growing mode in the PSM size
201 distribution, then the day was classified as "NPF with no growth". If there was no growing mode in
202 either size distribution, then the day was marked as "no NPF events". The definition is similar to Dada
203 et al. (2018) who used naturally charged ions to separate between NPF days with clustering only and
204 clustering plus visible growth. If there was a growing or an undefined new mode visible in the combined
205 size distribution but there was no clustering detected by the PSM, this day was marked as "unclear".
206 Days that lacked data from one of the instruments were marked as "no data".

207 **2.3.2 Condensation sink, nucleation and growth rate calculations**

208 The condensation sink and coagulation sink were calculated according to Dal Maso et al. (2005) from
209 the DMPS size distribution without any correction of aerosol hygroscopic behavior. Growth rates were
210 calculated using the maximum concentration method, in which we fit a Gaussian distribution to the
211 particle concentration evolution at a fixed size to determine the time of maximum concentration for a
212 given size channel in the HFDMPs. From these, the growth rate was calculated as the slope of a linear
213 least squares fit to the time-points of maximum concentration and their corresponding particle diameters.
214 The formation rates were calculated for several sizes by using the balance equation in Kulmala et al.
215 (2012) using the combined DMPS size-distributions (J_2 , J_3 , J_6) and the PSM plus combined DMPS size-
216 distribution ($J_{1.7}$).

217 **2.3.3 Mass spectrometer data analysis**

218 The APi-TOF and CI-APi-TOF data were analyzed using the Tofware package (v.3.1.0, Tofwerk,
219 Switzerland, and Aerodyne, USA) in the Igor Pro software (v.7.08, WaveMetrics, USA). The mass
220 accuracy is within 10 ppm (APi-TOF) and 5 ppm (CI-APi-TOF), and the mass resolutions were ~4500
221 (APi-TOF) and ~5000 (CI-APi-TOF) for ions >200 Th. Detailed information on the mass spectrometer



222 data analysis methods can be found in previous studies (Cai et al., 2022a; Cai et al., 2023a; Zha et al.,
223 2018; Zha et al., 2023; Fan et al., 2021).

224 **2.3.4 Kinetic model Simulations**

225 In order to evaluate the contribution of SA-amine clustering to cluster formation in the Po Valley, we
226 applied a kinetic model to simulate SA dimer concentrations. We simulated the cluster concentrations
227 and particle formation rates under different amine levels based on the model. The simulation was
228 performed with a temperature of 283 K, atmospheric pressure of 1.01×10^5 Pa, and the condensation
229 sink (CS) of 0.01 s^{-1} based on our measurement during the sampling period. In the model, the formation
230 rate of SA tetramer was regarded as the simulated particle formation rate. The standard molar Gibbs
231 free energy of formation and the corresponding evaporation of SA-amine clusters was based on
232 quantum chemistry with corrections from the experimental data. The detailed settings of the kinetic
233 model can be found in Cai et al. (2021).

234 **3. Results and discussions**

235 **3.1 NPF event frequency in Po Valley**

236 During the measurement period, frequent NPF events occurred in Po Valley (Fig. 2, Fig. S1). On 27%
237 of the days, we observed new particle formation with growth at the site, while on 39% of the days we
238 observed new particle formation without growth (Fig. S1). In total we observed new sub-3 nm clusters
239 forming on 66 % of the days. Even though we applied the similar definition of NPF events as previous
240 study, we can only compare our NPF events with growth type with the reported NPF event frequency
241 due to the lack of capacity to measure the sub-3nm particles in previous literature. Our results were
242 similar to those by Hamed et al. (2007) who observed NPF events on 36 % of the time in March and
243 April of 2002 at the same site. Manninen et al. (2010) observed NPF events during more than half of
244 all days from March to Oct in 2008 and Kontkanen et al. (2016) observed NPF during 89 % of the days
245 in July at the same site, which is higher than our observations. Hamed et al. (2007) also observed that
246 NPF with growth events on 60% of the days during summer, which suggests that summertime NPF
247 frequency at SPC is typically higher than our observation in springtime 2022. This difference in the
248 observed NPF was likely due to the different season with favorable conditions for NPF such as potential
249 lower CS (due to higher boundary layer mixing and less stagnant meteorological conditions) and higher
250 basic and organic molecule concentrations in summer. In addition, the abundant solar radiation and low
251 aerosol water content (limiting surface area and heterogenous reactions (Du et al., 2022)), likely create
252 favorable conditions for NPF to occur.

253 The median average particle formation rates at 1.7 nm, 3 nm and 7 nm for all sampling days with NPF
254 with growth events were $87 \text{ cm}^{-3} \text{ s}^{-1}$ ($32 - 133 \text{ cm}^{-3} \text{ s}^{-1}$), $3.2 \text{ cm}^{-3} \text{ s}^{-1}$ ($1.4 \text{ cm}^{-3} \text{ s}^{-1} - 7.0 \text{ cm}^{-3} \text{ s}^{-1}$) and 1.4
255 $\text{cm}^{-3} \text{ s}^{-1}$ ($0.3 \text{ cm}^{-3} \text{ s}^{-1} - 3.0 \text{ cm}^{-3} \text{ s}^{-1}$), respectively. The formation rate at 1.7 nm during NPF with growth
256 days (NPF with growth, $87 \text{ cm}^{-3} \text{ s}^{-1}$) is similar to that observed previously at the same site by Kontkanen
257 et al. (2016) in summer. The high formation rate, which is comparable with heavily polluted urban
258 environments such as Beijing and Shanghai, China ($59 \text{ cm}^{-3} \text{ s}^{-1} - 225 \text{ cm}^{-3} \text{ s}^{-1}$ (Deng et al., 2020; Yao
259 et al., 2018)), will be further discussed in section 3.4. The average formation rate ($J_{1.7}$) on NPF days
260 without growth ($24 \text{ cm}^{-3} \text{ s}^{-1}$) is much lower. During the noontime, the formation rate of particles for
261 NPF events with no growth was less than half of $J_{1.7}$ for NPF with growth (Fig. S2). It suggests that for
262 particles to grow in a polluted environment such as the Po Valley, there needs to be abundant clustering
263 to overcome losses to the existing condensation sink so that at least some of the particles survive to
264 grow into larger sizes.

265 **3.2 Nucleation mechanism**

266 Previous studies have demonstrated that SA is the most important gaseous precursor for NPF in
267 continental environments due to its extremely low volatility (Kirkby et al., 2011; Kulmala et al., 2013).
268 During the sampling period, high SA concentration was measured in the Po Valley, concurrent with the
269 frequent NPF events. The daily average concentration of SA was $4.6 \times 10^6 \text{ cm}^{-3}$ (10:00 – 14:00 LT),



270 similar to those in polluted megacities in China ($5 \times 10^6 \text{ cm}^{-3} - 7 \times 10^6 \text{ cm}^{-3}$). During the NPF with growth
271 days, the SA concentration was as high as $8.5 \times 10^6 \text{ cm}^{-3}$. The generally high concentrations were
272 consistent with a previous study conducted at the same site ($1.6 \times 10^7 \text{ cm}^{-3}$ during NPF in summer of
273 2009, (Paasonen et al., 2010)). For the entire sampling period, SA was moderately correlated with the
274 calculated $J_{1,7}$ ($r = 0.49$, Spearman correlation coefficient, for the logarithmic values) but varied among
275 different days. This suggests that in addition to SA, other components, such as basic molecules and
276 oxygenated organic molecules (OOMs), may also play a crucial role in driving NPF events and further
277 growth in the Po Valley.

278 To investigate the NPF mechanism in the Po Valley, in this study we firstly compared the
279 simultaneously measured $J_{1,7}$ and SA with recent Cosmics Leaving Outdoor Droplets (CLOUD)
280 chamber experiments that simulated NPF under polluted boundary layer conditions with anthropogenic
281 emissions (Xiao et al., 2021). In those experiments, amines, ammonia, as well as aromatics were added
282 to reflect a heavily anthropogenic emission-influenced environment. Certain basic molecules, including
283 amines (e.g., dimethylamine (DMA)) and ammonia (NH_3) have been shown to substantially enhance
284 nucleation and reduce evaporation by stabilizing atmospheric SA in chamber studies (Almeida et al.,
285 2013). Besides, OOMs can also contribute to NPF and subsequent particle growth, even without the
286 inclusion of SA (Kirkby et al., 2016; Xiao et al., 2021). As shown in Fig. 3a, most of the measurements
287 were above the SA- NH_3 system at 278K from the CLOUD chamber, suggesting the SA- NH_3 mechanism
288 itself cannot solely explain the measured $J_{1,7}$ and that other species are most likely participating to NPF
289 in the Po Valley. For instance, amines, such as DMA or TMA, with higher basicity may contribute to
290 NPF, consistent with not negligible concentrations of amines in previous studies in the aerosol at SPC
291 (Paglione et al., 2014; Decesari et al., 2014). For the whole sampling period, the median SA and $J_{1,7}$
292 values in Po Valley follows the SA-DMA- NH_3 (4 ppt DMA and 1ppb NH_3) and SA-DMA- NH_3 -Org
293 (adding additional oxidized aromatic organics (Xiao et al., 2021)) lines from the CLOUD chamber at
294 293K even though during most of the NPF days the average noontime temperature was around 285K
295 (Fig. 3a).

296 The SA dimer measured by CI-API-TOF is typically used as an indicator for the initial step for the
297 cluster formation in NPF events (Yan et al., 2021). According to a previous study (Yan et al., 2021),
298 the source and sink terms of the SA dimer can be determined by calculating the formation rate from SA
299 monomer collisions and the loss rate from the SA dimer through coagulation onto pre-existing particles
300 (Fig. 2b). In general, the correlation coefficient between SA dimer and its source to sink term ratios (r
301 = 0.80, Spearman correlation coefficient) indicated that similar to Chinese urban areas, SA dimer was
302 in a pseudo steady-state between the formation of SA monomer collision and the loss onto CS by
303 coagulation.

304 To further assess the influence of DMA, one of the most common and efficient base molecules for NPF
305 in urban environments (Yao et al., 2018), we compared the measured SA dimer concentrations with the
306 simulated ones under different DMA levels (from 0.1 ppt to reaching kinetic limit) by the kinetic model
307 (Fig. 3b). From our cluster kinetics simulations, during the peak hours of NPF, DMA concentrations
308 are expected to be in the range of 0.1 ppt to 5 ppt, which is lower than the need for reaching the kinetic
309 limit (Figs. 3b and S3). It implies that other factors, for example, the abundant ambient NH_3
310 concentrations (~ 10 ppb) or trimethylamine (TMA) during our study period may also participate in
311 cluster formation. It is consistent with the Vocus measurement, which suggests the ambient DMA
312 signals were close to the background levels (Fig. S4) even though it was difficult to quantify during the
313 campaign due to the absence of a suitable calibration method. The reason for not reaching SA-DMA
314 limit during the campaign could be 1) the relatively low emissions such as vehicle flows near our
315 sampling site that are reported to be the main sources for DMA in Chinese urban areas (Ge et al., 2011;
316 Zhu et al., 2022), 2) the nighttime high RH (85%) and daytime photolysis process quickly scavenge
317 gaseous DMA by wet deposition, heterogeneous reaction and photolysis (Leng et al., 2015; Yao et al.,



2016). Therefore, both of the abundant ambient NH_3 concentrations (~ 10 ppb) and amines likely participated in cluster formation during our study period.

Median particle growth rates (GR) during NPF events for 1.5 – 3 nm, 3 – 7 nm, 7 – 15 nm were 1.3 (1.0–2.4) nm h^{-1} , 4.6 (2.9 – 5.8) nm h^{-1} , and 5.1 (3.8 – 8.8) nm h^{-1} , respectively. The values in brackets represent the 25th and the 75th percentile of data (Fig. 3c). Growth rates increase with particle diameters, a phenomenon observed in other campaigns around the world as well (Kontkanen et al., 2017, Kulmala et al., 2013)) typically indicative of an increasing organic vapors contribution with size (e.g., Stolzenburg et al. (2018)). The growth rates observed here were similar to those observed by Kontkanen et al. (2016) at SPC in summer (7.2 nm h^{-1} for 7 – 20 nm) and our 1.5–3 nm growth rate matches well with Manninen et al. (2010) (1.5 nm h^{-1}) during spring in the Po Valley. A comparison to predicted growth rates from sulfuric acid condensation without organics, which was calculated based on kinetic collisions of the measured SA concentrations and the effect of van-der-Waals forces on the collision frequency ((Stolzenburg et al., 2020), Fig. 3c), suggests that sulfuric acid condensation may be on average sufficient for the growth of the smallest clusters (below 3 nm). It supports the argument that in the initial steps of NPF and growth in Po Valley sulfuric acid and its stabilizing molecules (likely the bases NH_3 and amines) were controlling particle formation. However, for particles to grow beyond 3 nm in size other vapors were needed, which was suggested by the significantly lower contribution of growth by SA (indicated by the green line) than the measured GR for 3 – 7 nm and 7 – 15 nm (Fig. 3c). Those vapors were likely a mixture of organics of anthropogenic and biogenic origin (with the latter emitted at higher rates during summer, which could cause the slightly higher values in Kontkanen et al. (2017)). We compared the GR during NPF with and without growth events using the method proposed in Kulmala et al. (2022) where the signal was averaged for all classified non-event days and then an appearance time fit was performed for each size channel independently, revealing also a growth pattern. We found no significant difference for the GR in 7 – 15 nm size range (GR=5.1 nm h^{-1} in NPF with growth days and average GR=6.1 nm h^{-1} in NPF without growth days). Considering the similar CS and GR levels for NPF with and without growth days, the higher formation rates at 1.7 nm (87 $\text{cm}^{-3} \text{s}^{-1}$) may be the decisive factor to overcome the CS and determine if a growing mode can be observed leading to a classification of the day as an NPF with growth day.

3.3 Ion and neutral clusters and further particle growth

During the campaign, we observed and identified different types of ion clusters with cluster ion measurements using the APi-TOF, including SA- NH_3 , SA-Amine, SA- NH_3 -Amine, SA- NH_3 -Org during NPF. In Fig. 4a, we presented the mass defect plot of the naturally charged ion clusters on April 20th, when strong NPF events were observed ($J_{1.7}$: 83 $\text{cm}^{-3} \text{s}^{-1}$). The presence of these clusters was usually in conjunction with SA tetramers (SA_4), pentamers (SA_5), and hexamers (SA_6), which potentially contribute to the NPF events. Acid-base clusters were not observed in monomer (SA_1), dimer (SA_2), or trimers (SA_3), likely due to declustering effects in the APi-TOF instrument (Cai et al., 2022b; Zha et al., 2023; Alfaouri et al., 2022).

Among all SA-base (SA-B) clusters, the most abundant SA- NH_3 clusters were from SA_4 -B to SA_6 -B (Fig. 4a), even though they are reported to more easily escape than DMA clusters due to collision-induced dissociation (Passananti et al., 2019). Pure SA-Amine clusters were only found in the SA_4 -B clusters with different types of amines, including methylamine (C_1 -amine), DMA (C_2 -amine), trimethylamine (C_3 -amine), and Butylamine (C_4 -amine). The detection of other SA-B than SA-DMA clusters indicates that other candidate bases could also play a crucial role in the complex atmosphere for nucleation. For example, a recent study conducted in Beijing highlights the importance of TMA that can accelerate the SA-DMA formation by 50% – 100% (Cai et al., 2023b). In the Po Valley, the signal intensity of SA_4 - NH_3 was significantly higher than that of the pure SA_4 -amine clusters (~ 2 times) even though amines (e.g., DMA) were proven to be more efficient (~ 3 orders of magnitude) than NH_3 in clustering (Almeida et al., 2013). It is different from Chinese cities such as Shanghai (Yao et al., 2018),



366 where high signals of SA₄-DMA clusters were found even with CI-APi-TOF which is more easy for
367 declustering.

368 SA-NH₃-Amine clusters could be found along with SA-NH₃ clusters in SA₅-B and SA₆-B. Similar
369 patterns of the high fractions of SA-NH₃ and SA-NH₃-Amine clusters were also reported in the CLOUD
370 chamber studies under relatively low DMA and high NH₃ conditions (Schobesberger et al., 2013).
371 Therefore, it can be concluded that a large amount of NH₃ also participates in NPF in the Po Valley
372 region. Meanwhile, with a much lower amount, amines may also play a crucial role in the formation of
373 small clusters (SA₄-B) due to their high stabilization efficiencies.

374 Moreover, some SA-NH₃-Org and I-containing ion clusters were also observed on NPF days, but to a
375 much lower extent than clusters involving NH₃ or DMA. It has been shown in previous CLOUD
376 chamber studies that the oxidation products of anthropogenic volatile organic compounds (AVOCs, e.g.,
377 naphthalene, trimethylbenzene and toluene) can largely promote the formation rate of particles (Xiao
378 et al., 2021). The I-containing ions (mainly IO₃⁻) likely originated from the Adriatic Sea during the
379 daytime, which was indicated by the easterly wind. Since no large iodine clusters were identified in the
380 APi-TOF (e.g., (HIO₃)₀₋₁(I₂O₅)_n-IO₃⁻, (He et al., 2021)), iodine-induced new particle formation in the
381 Po Valley may not be as important as the pristine marine environment (Sipila et al., 2016). During NPF
382 without growth days, the formation mechanism was similar to the NPF days regarding the ion cluster
383 measurement (Fig. S5).

384 Similar to polluted cities such as Beijing or Shanghai (Yan et al., 2021; Yao et al., 2018), the SA
385 monomer in the Po Valley can be observed during the peak hours (10:00 – 14:00 LT) in both NPF and
386 non-NPF days, but much lower SA dimer or trimers were found in the non-NPF days (Figs. 4b, and S6).
387 In the nighttime, the SA concentrations were close to zero due to the scavenging effect of hydrated
388 aerosol and hygroscopic growth of particles, as indicated by the high RH (Fig. 1). During our sampling
389 period, large amounts of organics were identified by the CI-APi-TOF. They were typically smaller than
390 400 Th with carbon numbers < 8 and oxygen numbers < 6 (Fig. S7). Due to the relatively high NO_x
391 levels (13 ppb) that can terminate the dimerization reactions (Yan et al., 2020), no OOM dimers were
392 found, which is different from clean and biogenically dominated environments such as Hyttiälä
393 (Lehtipalo et al., 2018). The compositions of OOMs were similar between NPF and non-NPF days but
394 with different abundance. Extremely high abundances of nitrophenols and their homologous
395 compounds were found on non-NPF days (~8 times higher than on NPF days), likely caused by both of
396 the enhanced primary (e.g., biomass burning (Mohr et al., 2013) and pesticide usage (Harrison et al.,
397 2005)) and secondary (e.g., photochemical and/or aqueous-phase secondary formation) sources (Zheng
398 et al., 2021; Gilardoni et al., 2016). C₂₋₄H_{4,5}N_{0,1}O_{3,4} compounds were found to be 50% higher (Fig. S7)
399 due to the higher RH during the non-NPF days and the enhanced heterogeneous reactions that form
400 smaller organics such as carboxylic acids. Previous studies also reported aqueous-phase organic aerosol
401 processing at high RH (Gilardoni et al., 2016) and high concentrations of carboxylic acids such as
402 formic, oxalic, and malonic acids in the springtime in the Po Valley (Saarikoski et al., 2012). In general,
403 the fraction of the abundance of nitrogen-containing OOMs (CHON) of total identified OOMs were 60%
404 – 70%, which is close to the levels reported in polluted cities such as Nanjing (Nie et al., 2022) and
405 Beijing (Guo et al., 2022). A slightly higher fraction of CHON compounds (73 %) was found during
406 non-NPF days than NPF days (67 %), consistent with higher NO_x and fine particulate matter levels
407 (Fig. S8). It is likely associated with the stagnant meteorological conditions and accumulation of
408 pollutants during the non-NPF days. However, the overall high amounts of CHON compounds and the
409 lack of organic dimers make it unlikely that OOMs drive the NPF process in the sub-3nm range (both
410 clustering and initial growth as no organic molecules of extremely- or ultra-low volatility were formed,
411 see e.g., Simon et al. (2020)). Their similar abundance on non-NPF and NPF days was also in line with
412 the similar estimated GR for both types of days.



413 3.4 Comparison between Po Valley and other environments

414

415 Even though the measured $J_{1.7}$ in Po Valley was at the same level of the values found in Chinese polluted
416 megacities, it was much higher than in clean environments, such as the boreal forest of Hyytiälä in
417 Finland, mountain sites Jungfrauoch in Switzerland, and Chacaltaya in Bolivia ($1.5 \text{ cm}^{-3} \text{ s}^{-1}$ – 2.0 cm^{-3}
418 s^{-1} , Fig. 5a). Similarly, the overall SA concentrations were similar to those in polluted megacities in
419 China (Fig. 5c), but much higher than those from the remote areas such as Hyytiälä ($9 \times 10^5 \text{ cm}^{-3}$) and
420 the Jungfrauoch ($5 \times 10^5 \text{ cm}^{-3}$). Compared to other remote sites, Chacaltaya has a higher SA
421 concentration ($2.3 \times 10^6 \text{ cm}^{-3}$) due to active volcanic degassing in the Andes (Zha et al., 2023). The SA
422 concentrations on NPF days ($8.6 \times 10^6 \text{ cm}^{-3}$) were twice as high as those during the non-NPF days (4
423 $\times 10^6 \text{ cm}^{-3}$), potentially associated with the higher RH and CS loss during the non-NPF days. This is
424 different from the findings from Beijing, where similar or even higher levels of SA during the non-NPF
425 days were found (Yan et al., 2021).

426 The overall CS in spring (median: $8.9 \times 10^{-3} \text{ s}^{-1}$) in the Po Valley was lower than that in other polluted
427 cities (1.5×10^{-1} – 2.0 s^{-1}), but significantly higher than that in clean environments ($2.0 \times 10^{-4} \text{ s}^{-1}$ (Hyytiälä
428 and Jungfrauoch) – $3.0 \times 10^{-3} \text{ s}^{-1}$ (Chacaltaya with the influence of volcanoes), Fig. 5e). Contrary to
429 Beijing or Shanghai where CS levels and efficiencies are the dominant factors for the NPF process (Du
430 et al., 2022), no strong influence of CS was found between NPF and non-NPF days in the Po Valley,
431 and only slightly higher CS was found during the noontime of non-NPF days (median: $9.4 \times 10^{-3} \text{ s}^{-1}$) than
432 NPF days (median: $8.6 \times 10^{-3} \text{ s}^{-1}$). It is likely associated with the general lower CS than the Chinese
433 megacities. The observed growth rate for 7 – 15 nm particles in the Po Valley was about 5.1 nm h^{-1} ,
434 comparable to other urban and remote sites (2.9 – 9.1 nm h^{-1} , Fig. 5f). The general similar growth rates
435 among different types of environments were also reported in previous studies (Deng et al., 2020), which
436 needs further investigation in future research.

437 For the basic gaseous precursors, the average concentration of NH_3 was ~ 10 ppb, which was in the same
438 range as that found in the Chinese megacities (10 – 30 ppb) and much higher than that at remote sites
439 (< 0.1 ppb, Table S1). The high NH_3 can be attributed to agricultural activities such as fertilization,
440 which were widely applied during springtime in the region. The strong interference of ammonia emitted
441 from fertilization to NPF was also observed in Qvidja, an agricultural site in Southern Finland (Olin et
442 al., 2022). During our sampling period, measured DMA were too close to the detection limit of the
443 Vocus (Fig. S2), and lower than those observed in the Chinese megacities (10 – 40 ppt, Fig. 5d). In the
444 spring season, DMA in the Po Valley cannot fully stabilize all atmospheric SA clusters and hence NPF
445 is very sensitive to variations in the concentrations of the different stabilizers (NH_3 , DMA, and as shown
446 by our analysis likely only to a lower extent organics). This could explain the scattered correlation
447 between the formation rate and SA concentrations on different days (Fig. 3).

448 Therefore, it can be concluded that the high sulfuric acid concentrations, basic molecules and formation
449 rates may be the reason for the high frequency of NPF events in the Po Valley region. The abundant
450 organics led to a comparable GR to Chinese megacities such as Beijing and Shanghai. Due to the
451 relatively lower CS than these megacities, the newly formed particles may however have a higher
452 survival probability compared to the megacities and provide more long-term surviving particles in the
453 Po Valley, indicating a decisive role of NPF for Po-Valley aerosol and $\text{PM}_{2.5}$ concentrations.

454 4. Conclusions

455 In this study, we conducted a continuous two-month measurement campaign of the chemical
456 composition and physical properties of newly formed particles and clusters in the Italian Po Valley
457 during springtime. The Po Valley experienced frequent NPF events during the sampling period,
458 occurring on approximately 66% of the days. We observed high concentrations of sulfuric acid during
459 the NPF events, comparable to those found in Chinese megacities. The correlation between the
460 formation rate of particles and sulfuric acid concentrations, together with the information from
461 dimethylamine simulations and CLOUD chamber experiments, suggest that gaseous DMA might have



462 been insufficient to stabilize all atmospheric sulfuric acid during our sampling period. Except for DMA,
463 other amines and NH_3 were also involved in NPF in the Po Valley, which was supported by the high
464 abundance of SA- NH_3 and SA-amine- NH_3 clusters measured by the API-TOF on NPF days. Generally,
465 the NPF mechanism is therefore very sensitive to the abundance of amines (e.g., DMA) with high levels
466 of NH_3 , resulting in a more scattered correlation between H_2SO_4 concentrations and measured formation
467 rate. At the same time, OOMs do not seem to be decisive for the sub-3 nm formation process due to the
468 lack of ultra-low volatility organics (highly oxygenated CHO compounds and dimers), however low
469 volatility organics were abundant enough to induce fast growth processes above 3 nm. The comparable
470 GR and formation rate, but lower CS compared to other polluted environments, indicate a high survival
471 probability for the newly formed particles. Therefore, NPF is likely to play an important role in the fine
472 particle concentrations and pollution levels in the Po Valley region.

473 **Data availability**

474 Data are available from the authors upon request.

475 **Competing interests**

476 At least one of the (co-)authors is a member of the editorial board of Atmospheric Chemistry and
477 Physics

478 **Author contributions**

479 JC, DS, FB, and MK designed the research. JC, JS, YFG, SH, MP, AN, FM, SD, MR, NZ and CM
480 collected the data at the SPC site. JC, JS, YG, ST, RY, DA, QZ, DS and FB interpreted the data. MP,
481 WH, YL, GC, LQ, KL, YG, CW, WN, CM, QZ, DS, FB helped to improve the manuscript. JC, JS, DS,
482 and FB wrote the manuscript with contributions from all co-authors. All authors have given approval
483 to the final version of this manuscript.

484 **Acknowledgements**

485 The work is supported by the Academy of Finland (Center of Excellence in Atmospheric Sciences,
486 project no. 307331, PROF13 funding no. 311932, and ACCC Flagship no. 337549), the European
487 Research Council via ATM-GTP (no. 742206), Consolidator grant INTEGRATE (no. 865799) and
488 CHAPAs (no. 850614), the European Union's Horizon 2020 research and innovation programme
489 (project FORCeS under grant agreement no. 821205, H2020-INFRAIA-2020-1 grant agreement no.
490 101008004, Marie Skłodowska–Curie grant agreement no. 895875 (NPF-PANDA), the Vienna Science
491 and Technology Fund (WWTF) through project VRG22-003, Jenny and Antti Wihuri Foundation, and
492 the Knut and Alice Wallenberg Foundation (WAF project CLOUDFORM, grant no. 2017.0165). The
493 authors also would like to thank the effort from all the researchers in the SPC site. The authors would
494 also like to thank Chenjuan Deng, Mao Xiao and Lubna Dada for providing the supporting data in
495 Beijing and CLOUD chamber experiment.

496



497 **Reference**

- 498 Alfaouri, D., Passananti, M., Zanca, T., Ahonen, L., Kangasluoma, J., Kubečka, J., Myllys, N., and
499 Vehkamäki, H.: A study on the fragmentation of sulfuric acid and dimethylamine clusters inside an
500 atmospheric pressure interface time-of-flight mass spectrometer, *Atmospheric Measurement*
501 *Techniques*, 15, 11-19, 10.5194/amt-15-11-2022, 2022.
- 502 Almeida, J., Schobesberger, S., Kurten, A., Ortega, I. K., Kupiainen-Maatta, O., Praplan, A. P., Adamov,
503 A., Amorim, A., Bianchi, F., Breitenlechner, M., David, A., Dommen, J., Donahue, N. M., Downard, A.,
504 Dunne, E., Duplissy, J., Ehrhart, S., Flagan, R. C., Franchin, A., Guida, R., Hakala, J., Hansel, A., Heinritzi,
505 M., Henschel, H., Jokinen, T., Junninen, H., Kajos, M., Kangasluoma, J., Keskinen, H., Kupc, A., Kurten,
506 T., Kvashin, A. N., Laaksonen, A., Lehtipalo, K., Leiminger, M., Leppa, J., Loukonen, V., Makhmutov, V.,
507 Mathot, S., McGrath, M. J., Nieminen, T., Olenius, T., Onnela, A., Petaja, T., Riccobono, F., Riipinen, I.,
508 Rissanen, M., Rondo, L., Ruuskanen, T., Santos, F. D., Sarnela, N., Schallhart, S., Schnitzhofer, R.,
509 Seinfeld, J. H., Simon, M., Sipila, M., Stozhkov, Y., Stratmann, F., Tome, A., Trostl, J., Tsagkogeorgas, G.,
510 Vaattovaara, P., Viisanen, Y., Virtanen, A., Vrtala, A., Wagner, P. E., Weingartner, E., Wex, H.,
511 Williamson, C., Wimmer, D., Ye, P., Yli-Juuti, T., Carslaw, K. S., Kulmala, M., Curtius, J., Baltensperger,
512 U., Worsnop, D. R., Vehkamäki, H., and Kirkby, J.: Molecular understanding of sulphuric acid-amine
513 particle nucleation in the atmosphere, *Nature*, 502, 359-363, 10.1038/nature12663, 2013.
- 514 Boulon, J., Sellegri, K., Venzac, H., Picard, D., Weingartner, E., Wehrle, G., Collaud Coen, M., Bütikofer,
515 R., Flückiger, E., Baltensperger, U., and Laj, P.: New particle formation and ultrafine charged aerosol
516 climatology at a high altitude site in the Alps (Jungfraujoch, 3580 m a.s.l., Switzerland), *Atmospheric*
517 *Chemistry and Physics*, 10, 9333-9349, 10.5194/acp-10-9333-2010, 2010.
- 518 Brean, J., Beddows, D. C. S., Shi, Z., Temime-Roussel, B., Marchand, N., Querol, X., Alastuey, A.,
519 Minguillón, M. C., and Harrison, R. M.: Molecular insights into new particle formation in Barcelona,
520 Spain, *Atmospheric Chemistry and Physics*, 20, 10029-10045, 10.5194/acp-20-10029-2020, 2020.
- 521 Cai, J., Daellenbach, K. R., Wu, C., Zheng, Y., Zheng, F., Du, W., Haslett, S. L., Chen, Q., Kulmala, M., and
522 Mohr, C.: Characterization of offline analysis of particulate matter with FIGAERO-CIMS, *Atmospheric*
523 *Measurement Techniques*, 16, 1147-1165, 10.5194/amt-16-1147-2023, 2023a.
- 524 Cai, J., Wu, C., Wang, J., Du, W., Zheng, F., Hakala, S., Fan, X., Chu, B., Yao, L., Feng, Z., Liu, Y., Sun, Y.,
525 Zheng, J., Yan, C., Bianchi, F., Kulmala, M., Mohr, C., and Daellenbach, K. R.: Influence of organic
526 aerosol molecular composition on particle absorptive properties in autumn Beijing, *Atmospheric*
527 *Chemistry and Physics*, 22, 1251-1269, 10.5194/acp-22-1251-2022, 2022a.
- 528 Cai, R., Yin, R., Li, X., Xie, H.-B., Yang, D., Kerminen, V.-M., Smith, J. N., Ma, Y., Hao, J., Chen, J., Kulmala,
529 M., Zheng, J., Jiang, J., and Elm, J.: Significant contributions of trimethylamine to sulfuric acid
530 nucleation in polluted environments, *npj Climate and Atmospheric Science*, 6, 10.1038/s41612-023-
531 00405-3, 2023b.
- 532 Cai, R., Yan, C., Yang, D., Yin, R., Lu, Y., Deng, C., Fu, Y., Ruan, J., Li, X., Kontkanen, J., Zhang, Q.,
533 Kangasluoma, J., Ma, Y., Hao, J., Worsnop, D. R., Bianchi, F., Paasonen, P., Kerminen, V. M., Liu, Y.,
534 Wang, L., Zheng, J., Kulmala, M., and Jiang, J.: Sulfuric acid-amine nucleation in urban Beijing, *Atmos.*
535 *Chem. Phys.*, 21, 2457-2468, 10.5194/acp-21-2457-2021, 2021.
- 536 Cai, R., Yin, R., Yan, C., Yang, D., Deng, C., Dada, L., Kangasluoma, J., Kontkanen, J., Halonen, R., Ma, Y.,
537 Zhang, X., Paasonen, P., Petaja, T., Kerminen, V. M., Liu, Y., Bianchi, F., Zheng, J., Wang, L., Hao, J.,
538 Smith, J. N., Donahue, N. M., Kulmala, M., Worsnop, D. R., and Jiang, J.: The missing base molecules in
539 atmospheric acid-base nucleation, *Natl Sci Rev*, 9, nwac137, 10.1093/nsr/nwac137, 2022b.
- 540 Chu, B., Kerminen, V.-M., Bianchi, F., Yan, C., Petäjä, T., and Kulmala, M.: Atmospheric new particle
541 formation in China, *Atmospheric Chemistry and Physics*, 19, 115-138, 10.5194/acp-19-115-2019, 2019.
- 542 Dada, L., Chellapermal, R., Buenostro Mazon, S., Paasonen, P., Lampilahti, J., Manninen, H. E.,
543 Junninen, H., Petäjä, T., Kerminen, V.-M., and Kulmala, M.: Refined classification and characterization
544 of atmospheric new-particle formation events using air ions, *Atmospheric Chemistry and Physics*, 18,
545 17883-17893, 10.5194/acp-18-17883-2018, 2018.
- 546 Daellenbach, K. R., Manousakas, M., Jiang, J., Cui, T., Chen, Y., El Haddad, I., Fermo, P., Colombi, C.,
547 and Prévôt, A. S. H.: Organic aerosol sources in the Milan metropolitan area – Receptor modelling



548 based on field observations and air quality modelling, *Atmospheric Environment*, 119799,
549 <https://doi.org/10.1016/j.atmosenv.2023.119799>, 2023.

550 Dal Maso, M., Kulmala, M., Riipinen, I., Wagner, R., Hussein, T., Aalto, P. P., and Lehtinen, K. E. J.:
551 Formation and growth of fresh atmospheric aerosols: eight years of aerosol size distribution data from
552 SMEAR II, Hyytiälä, Finland, *Boreal Environment Research*, 10, 323-336, 2005.

553 de Jesus, A. L., Rahman, M. M., Mazaheri, M., Thompson, H., Knibbs, L. D., Jeong, C., Evans, G., Nei,
554 W., Ding, A., Qiao, L., Li, L., Portin, H., Niemi, J. V., Timonen, H., Luoma, K., Petaja, T., Kulmala, M.,
555 Kowalski, M., Peters, A., Cyrus, J., Ferrero, L., Manigrasso, M., Avino, P., Buonano, G., Reche, C., Querol,
556 X., Beddows, D., Harrison, R. M., Sowlat, M. H., Sioutas, C., and Morawska, L.: Ultrafine particles and
557 PM(2.5) in the air of cities around the world: Are they representative of each other?, *Environ Int*, 129,
558 118-135, 10.1016/j.envint.2019.05.021, 2019.

559 Decesari, S., Allan, J., Plass-Duelmer, C., Williams, B. J., Paglione, M., Facchini, M. C., O'Dowd, C.,
560 Harrison, R. M., Gietl, J. K., Coe, H., Giulianelli, L., Gobbi, G. P., Lanconelli, C., Carbone, C., Worsnop,
561 D., Lambe, A. T., Ahern, A. T., Moretti, F., Tagliavini, E., Elste, T., Gilge, S., Zhang, Y., and Dall'Osto, M.:
562 Measurements of the aerosol chemical composition and mixing state in the Po Valley using multiple
563 spectroscopic techniques, *Atmospheric Chemistry and Physics*, 14, 12109-12132, 10.5194/acp-14-
564 12109-2014, 2014.

565 Deng, C., Fu, Y., Dada, L., Yan, C., Cai, R., Yang, D., Zhou, Y., Yin, R., Lu, Y., Li, X., Qiao, X., Fan, X., Nie,
566 W., Kontkanen, J., Kangasluoma, J., Chu, B., Ding, A., Kerminen, V. M., Paasonen, P., Worsnop, D. R.,
567 Bianchi, F., Liu, Y., Zheng, J., Wang, L., Kulmala, M., and Jiang, J.: Seasonal Characteristics of New
568 Particle Formation and Growth in Urban Beijing, *Environ Sci Technol*, 54, 8547-8557,
569 10.1021/acs.est.0c00808, 2020.

570 Du, W., Cai, J., Zheng, F., Yan, C., Zhou, Y., Guo, Y., Chu, B., Yao, L., Heikkinen, L. M., Fan, X., Wang, Y.,
571 Cai, R., Hakala, S., Chan, T., Kontkanen, J., Tuovinen, S., Petäjä, T., Kangasluoma, J., Bianchi, F.,
572 Paasonen, P., Sun, Y., Kerminen, V.-M., Liu, Y., Daellenbach, K. R., Dada, L., and Kulmala, M.: Influence
573 of Aerosol Chemical Composition on Condensation Sink Efficiency and New Particle Formation in
574 Beijing, *Environmental Science & Technology Letters*, 9, 375-382, 10.1021/acs.estlett.2c00159, 2022.

575 Fan, X., Cai, J., Yan, C., Zhao, J., Guo, Y., Li, C., Dällenbach, K. R., Zheng, F., Lin, Z., Chu, B., Wang, Y.,
576 Dada, L., Zha, Q., Du, W., Kontkanen, J., Kurtén, T., Iyer, S., Kujansuu, J. T., Petäjä, T., Worsnop, D. R.,
577 Kerminen, V.-M., Liu, Y., Bianchi, F., Tham, Y. J., Yao, L., and Kulmala, M.: Atmospheric gaseous
578 hydrochloric and hydrobromic acid in urban Beijing, China: detection, source identification and
579 potential atmospheric impacts, *Atmospheric Chemistry and Physics*, 21, 11437-11452, 10.5194/acp-
580 21-11437-2021, 2021.

581 Fernández de la Mora, J. and Kozlowski, J.: Hand-held differential mobility analyzers of high resolution
582 for 1–30nm particles: Design and fabrication considerations, *Journal of Aerosol Science*, 57, 45-53,
583 10.1016/j.jaerosci.2012.10.009, 2013.

584 Finzi, G. and Tebaldi, G.: A mathematical model for air pollution forecast and alarm in an urban area,
585 *Atmospheric Environment* (1967), 16, 2055-2059, [https://doi.org/10.1016/0004-6981\(82\)90276-1](https://doi.org/10.1016/0004-6981(82)90276-1),
586 1982.

587 Ge, X., Wexler, A. S., and Clegg, S. L.: Atmospheric amines – Part I. A review, *Atmospheric Environment*,
588 45, 524-546, <https://doi.org/10.1016/j.atmosenv.2010.10.012>, 2011.

589 Gilardoni, S., Massoli, P., Paglione, M., Giulianelli, L., Carbone, C., Rinaldi, M., Decesari, S., Sandrini, S.,
590 Costabile, F., Gobbi, G. P., Pietrogrande, M. C., Visentin, M., Scotto, F., Fuzzi, S., and Facchini, M. C.:
591 Direct observation of aqueous secondary organic aerosol from biomass-burning emissions, *Proc Natl
592 Acad Sci U S A*, 113, 10013-10018, 10.1073/pnas.1602212113, 2016.

593 Guo, S., Hu, M., Peng, J., Wu, Z., Zamora, M. L., Shang, D., Du, Z., Zheng, J., Fang, X., Tang, R., Wu, Y.,
594 Zeng, L., Shuai, S., Zhang, W., Wang, Y., Ji, Y., Li, Y., Zhang, A. L., Wang, W., Zhang, F., Zhao, J., Gong,
595 X., Wang, C., Molina, M. J., and Zhang, R.: Remarkable nucleation and growth of ultrafine particles
596 from vehicular exhaust, *Proceedings of the National Academy of Sciences*, 10.1073/pnas.1916366117,
597 2020.



598 Guo, Y., Yan, C., Liu, Y., Qiao, X., Zheng, F., Zhang, Y., Zhou, Y., Li, C., Fan, X., Lin, Z., Feng, Z., Zhang, Y.,
599 Zheng, P., Tian, L., Nie, W., Wang, Z., Huang, D., Daellenbach, K. R., Yao, L., Dada, L., Bianchi, F., Jiang,
600 J., Liu, Y., Kerminen, V.-M., and Kulmala, M.: Seasonal variation in oxygenated organic molecules in
601 urban Beijing and their contribution to secondary organic aerosol, *Atmospheric Chemistry and Physics*,
602 22, 10077-10097, 10.5194/acp-22-10077-2022, 2022.

603 Hamed, A., Joutsensaari, J., Mikkonen, S., Sogacheva, L., Dal Maso, M., Kulmala, M., Cavalli, F., Fuzzi,
604 S., Facchini, M. C., Decesari, S., Mircea, M., Lehtinen, K. E. J., and Laaksonen, A.: Nucleation and growth
605 of new particles in Po Valley, Italy, *Atmos. Chem. Phys.*, 7, 355-376, 10.5194/acp-7-355-2007, 2007.

606 Harrison, M. A. J., Barra, S., Borghesi, D., Vione, D., Arsene, C., and Iulian Olariu, R.: Nitrated phenols
607 in the atmosphere: a review, *Atmospheric Environment*, 39, 231-248,
608 10.1016/j.atmosenv.2004.09.044, 2005.

609 He, X. C., Tham, Y. J., Dada, L., Wang, M., Finkenzeller, H., Stolzenburg, D., Iyer, S., Simon, M., Kurten,
610 A., Shen, J., Rorup, B., Rissanen, M., Schobesberger, S., Baalbaki, R., Wang, D. S., Koenig, T. K., Jokinen,
611 T., Sarnela, N., Beck, L. J., Almeida, J., Amanatidis, S., Amorim, A., Ataei, F., Baccharini, A., Bertozzi, B.,
612 Bianchi, F., Brilke, S., Caudillo, L., Chen, D., Chiu, R., Chu, B., Dias, A., Ding, A., Dommen, J., Duplissy, J.,
613 El Haddad, I., Gonzalez Carracedo, L., Granzin, M., Hansel, A., Heinritzi, M., Hofbauer, V., Junninen, H.,
614 Kangasluoma, J., Kempainen, D., Kim, C., Kong, W., Krechmer, J. E., Kvashin, A., Laitinen, T.,
615 Lamkaddam, H., Lee, C. P., Lehtipalo, K., Leiminger, M., Li, Z., Makhmutov, V., Manninen, H. E., Marie,
616 G., Marten, R., Mathot, S., Mauldin, R. L., Mentler, B., Mohler, O., Muller, T., Nie, W., Onnela, A., Petaja,
617 T., Pfeifer, J., Philippov, M., Ranjithkumar, A., Saiz-Lopez, A., Salma, I., Scholz, W., Schuchmann, S.,
618 Schulze, B., Steiner, G., Stozhkov, Y., Tauber, C., Tome, A., Thakur, R. C., Vaisanen, O., Vazquez-Pufleau,
619 M., Wagner, A. C., Wang, Y., Weber, S. K., Winkler, P. M., Wu, Y., Xiao, M., Yan, C., Ye, Q., Ylisirnio, A.,
620 Zauner-Wieczorek, M., Zha, Q., Zhou, P., Flagan, R. C., Curtius, J., Baltensperger, U., Kulmala, M.,
621 Kerminen, V. M., Kurten, T., Donahue, N. M., Volkamer, R., Kirkby, J., Worsnop, D. R., and Sipila, M.:
622 Role of iodine oxoacids in atmospheric aerosol nucleation, *Science*, 371, 589-595,
623 10.1126/science.abe0298, 2021.

624 Jokinen, T., Sipilä, M., Junninen, H., Ehn, M., Lönn, G., Hakala, J., Petäjä, T., Mauldin, R. L., Kulmala, M.,
625 and Worsnop, D. R.: Atmospheric sulphuric acid and neutral cluster measurements using CI-API-TOF,
626 *Atmospheric Chemistry and Physics*, 12, 4117-4125, 10.5194/acp-12-4117-2012, 2012.

627 Junninen, H., Ehn, M., Petäjä, T., Luosujärvi, L., Kotiaho, T., Kostianen, R., Rohner, U., Gonin, M.,
628 Fuhrer, K., Kulmala, M., and Worsnop, D. R.: A high-resolution mass spectrometer to measure
629 atmospheric ion composition, *Atmospheric Measurement Techniques*, 3, 1039-1053, 10.5194/amt-3-
630 1039-2010, 2010.

631 Kangasluoma, J., Ahonen, L. R., Laurila, T. M., Cai, R., Enroth, J., Mazon, S. B., Korhonen, F., Aalto, P.
632 P., Kulmala, M., Attoui, M., and Petäjä, T.: Laboratory verification of a new high flow differential
633 mobility particle sizer, and field measurements in Hyytiälä, *Journal of Aerosol Science*, 124, 1-9,
634 10.1016/j.jaerosci.2018.06.009, 2018.

635 Kirkby, J., Curtius, J., Almeida, J., Dunne, E., Duplissy, J., Ehrhart, S., Franchin, A., Gagne, S., Ickes, L.,
636 Kurten, A., Kupc, A., Metzger, A., Riccobono, F., Rondo, L., Schobesberger, S., Tsagkogeorgas, G.,
637 Wimmer, D., Amorim, A., Bianchi, F., Breitenlechner, M., David, A., Dommen, J., Downard, A., Ehn, M.,
638 Flagan, R. C., Haider, S., Hansel, A., Hauser, D., Jud, W., Junninen, H., Kreissl, F., Kvashin, A., Laaksonen,
639 A., Lehtipalo, K., Lima, J., Lovejoy, E. R., Makhmutov, V., Mathot, S., Mikkilä, J., Minginette, P., Mogo,
640 S., Nieminen, T., Onnela, A., Pereira, P., Petaja, T., Schnitzhofer, R., Seinfeld, J. H., Sipilä, M., Stozhkov,
641 Y., Stratmann, F., Tome, A., Vanhanen, J., Viisanen, Y., Vrtala, A., Wagner, P. E., Walther, H.,
642 Weingartner, E., Wex, H., Winkler, P. M., Carslaw, K. S., Worsnop, D. R., Baltensperger, U., and Kulmala,
643 M.: Role of sulphuric acid, ammonia and galactic cosmic rays in atmospheric aerosol nucleation,
644 *Nature*, 476, 429-433, 10.1038/nature10343, 2011.

645 Kirkby, J., Duplissy, J., Sengupta, K., Frege, C., Gordon, H., Williamson, C., Heinritzi, M., Simon, M., Yan,
646 C., Almeida, J., Trostl, J., Nieminen, T., Ortega, I. K., Wagner, R., Adamov, A., Amorim, A., Bernhammer,
647 A. K., Bianchi, F., Breitenlechner, M., Brilke, S., Chen, X., Craven, J., Dias, A., Ehrhart, S., Flagan, R. C.,
648 Franchin, A., Fuchs, C., Guida, R., Hakala, J., Hoyle, C. R., Jokinen, T., Junninen, H., Kangasluoma, J.,



- 649 Kim, J., Krapf, M., Kurten, A., Laaksonen, A., Lehtipalo, K., Makhmutov, V., Mathot, S., Molteni, U.,
650 Onnela, A., Perakyla, O., Piel, F., Petaja, T., Praplan, A. P., Pringle, K., Rap, A., Richards, N. A., Riipinen,
651 I., Rissanen, M. P., Rondo, L., Sarnela, N., Schobesberger, S., Scott, C. E., Seinfeld, J. H., Sipila, M.,
652 Steiner, G., Stozhkov, Y., Stratmann, F., Tome, A., Virtanen, A., Vogel, A. L., Wagner, A. C., Wagner, P.
653 E., Weingartner, E., Wimmer, D., Winkler, P. M., Ye, P., Zhang, X., Hansel, A., Dommen, J., Donahue, N.
654 M., Worsnop, D. R., Baltensperger, U., Kulmala, M., Carslaw, K. S., and Curtius, J.: Ion-induced
655 nucleation of pure biogenic particles, *Nature*, 533, 521-526, 10.1038/nature17953, 2016.
- 656 Kontkanen, J., Järvinen, E., Manninen, H. E., Lehtipalo, K., Kangasluoma, J., Decesari, S., Gobbi, G. P.,
657 Laaksonen, A., Petäjä, T., and Kulmala, M.: High concentrations of sub-3nm clusters and frequent new
658 particle formation observed in the Po Valley, Italy, during the PEGASOS 2012 campaign, *Atmospheric
659 Chemistry and Physics*, 16, 1919-1935, 10.5194/acp-16-1919-2016, 2016.
- 660 Kontkanen, J., Lehtipalo, K., Ahonen, L., Kangasluoma, J., Manninen, H. E., Hakala, J., Rose, C., Sellegri,
661 K., Xiao, S., Wang, L., Qi, X., Nie, W., Ding, A., Yu, H., Lee, S., Kerminen, V.-M., Petäjä, T., and Kulmala,
662 M.: Measurements of sub-3 nm particles using a particle size magnifier in different environments:
663 from clean mountain top to polluted megacities, *Atmospheric Chemistry and Physics*, 17, 2163-2187,
664 10.5194/acp-17-2163-2017, 2017.
- 665 Kulmala, M., Kerminen, V. M., Petäjä, T., Ding, A. J., and Wang, L.: Atmospheric gas-to-particle
666 conversion: why NPF events are observed in megacities?, *Faraday Discussions*, 200, 271-288,
667 10.1039/C6FD00257A, 2017.
- 668 Kulmala, M., Petäjä, T., Nieminen, T., Sipilä, M., Manninen, H. E., Lehtipalo, K., Dal Maso, M., Aalto, P.
669 P., Junninen, H., Paasonen, P., Riipinen, I., Lehtinen, K. E. J., Laaksonen, A., and Kerminen, V.-M.:
670 Measurement of the nucleation of atmospheric aerosol particles, *Nature Protocols*, 7, 1651-1667,
671 10.1038/nprot.2012.091, 2012.
- 672 Kulmala, M., Junninen, H., Dada, L., Salma, I., Weidinger, T., Thén, W., Vörösmarty, M., Komsaare, K.,
673 Stolzenburg, D., Cai, R., Yan, C., Li, X., Deng, C., Jiang, J., Petäjä, T., Nieminen, T., and Kerminen, V.-M.:
674 Quiet New Particle Formation in the Atmosphere, *Frontiers in Environmental Science*, 10,
675 10.3389/fenvs.2022.912385, 2022.
- 676 Kulmala, M., Kontkanen, J., Junninen, H., Lehtipalo, K., Manninen, H. E., Nieminen, T., Petäjä, T., Sipilä,
677 M., Schobesberger, S., Rantala, P., Franchin, A., Jokinen, T., Järvinen, E., Äijälä, M., Kangasluoma, J.,
678 Hakala, J., Aalto, P. P., Paasonen, P., Mikkilä, J., Vanhanen, J., Aalto, J., Hakola, H., Makkonen, U.,
679 Ruuskanen, T., Mauldin, R. L., Duplissy, J., Vehkamäki, H., Bäck, J., Kortelainen, A., Riipinen, I., Kurtén,
680 T., Johnston, M. V., Smith, J. N., Ehn, M., Mentel, T. F., Lehtinen, K. E. J., Laaksonen, A., Kerminen, V.-
681 M., and Worsnop, D. R.: Direct Observations of Atmospheric Aerosol Nucleation, *Science*, 339, 943-
682 946, 10.1126/science.1227385, 2013.
- 683 Kulmala, M., Dada, L., Daellenbach, K. R., Yan, C., Stolzenburg, D., Kontkanen, J., Ezhova, E., Hakala, S.,
684 Tuovinen, S., Kokkonen, T. V., Kurppa, M., Cai, R., Zhou, Y., Yin, R., Baalbaki, R., Chan, T., Chu, B., Deng,
685 C., Fu, Y., Ge, M., He, H., Heikkinen, L., Junninen, H., Liu, Y., Lu, Y., Nie, W., Rusanen, A., Vakkari, V.,
686 Wang, Y., Yang, G., Yao, L., Zheng, J., Kujansuu, J., Kangasluoma, J., Petaja, T., Paasonen, P., Jarvi, L.,
687 Worsnop, D., Ding, A., Liu, Y., Wang, L., Jiang, J., Bianchi, F., and Kerminen, V. M.: Is reducing new
688 particle formation a plausible solution to mitigate particulate air pollution in Beijing and other Chinese
689 megacities?, *Faraday Discuss*, 226, 334-347, 10.1039/d0fd00078g, 2021.
- 690 Kurten, A., Rondo, L., Ehrhart, S., and Curtius, J.: Calibration of a chemical ionization mass
691 spectrometer for the measurement of gaseous sulfuric acid, *J Phys Chem A*, 116, 6375-6386,
692 10.1021/jp212123n, 2012.
- 693 Lampimäki, M., Baalbaki, R., Ahonen, L., Korhonen, F., Cai, R., Chan, T., Stolzenburg, D., Petäjä, T.,
694 Kangasluoma, J., Vanhanen, J., and Lehtipalo, K.: Novel aerosol diluter – Size dependent
695 characterization down to 1 nm particle size, *Journal of Aerosol Science*, 172, 106180,
696 <https://doi.org/10.1016/j.jaerosci.2023.106180>, 2023.
- 697 Lehtipalo, K., Ahonen, L. R., Baalbaki, R., Sulo, J., Chan, T., Laurila, T., Dada, L., Duplissy, J., Miettinen,
698 E., Vanhanen, J., Kangasluoma, J., Kulmala, M., Petäjä, T., and Jokinen, T.: The standard operating



- 699 procedure for Airmodus Particle Size Magnifier and nano-Condensation Nucleus Counter, *Journal of*
700 *Aerosol Science*, 159, 10.1016/j.jaerosci.2021.105896, 2022.
- 701 Lehtipalo, K., Yan, C., Dada, L., Bianchi, F., Xiao, M., Wagner, R., Stolzenburg, D., Ahonen, L. R., Amorim,
702 A., Baccharini, A., Bauer, P. S., Baumgartner, B., Bergen, A., Bernhammer, A.-K., Breitenlechner, M.,
703 Brilke, S., Buchholz, A., Mazon, S. B., Chen, D., Chen, X., Dias, A., Dommen, J., Draper, D. C., Duplissy,
704 J., Ehn, M., Finkenzeller, H., Fischer, L., Frege, C., Fuchs, C., Garmash, O., Gordon, H., Hakala, J., He, X.,
705 Heikkinen, L., Heinritzi, M., Helm, J. C., Hofbauer, V., Hoyle, C. R., Jokinen, T., Kangasluoma, J.,
706 Kerminen, V.-M., Kim, C., Kirkby, J., Kontkanen, J., Kürten, A., Lawler, M. J., Mai, H., Mathot, S., Mauldin,
707 R. L., Molteni, U., Nichman, L., Nie, W., Nieminen, T., Ojdanic, A., Onnela, A., Passananti, M., Petäjä,
708 T., Piel, F., Pospisilova, V., Quéléver, L. L. J., Rissanen, M. P., Rose, C., Sarnela, N., Schallhart, S.,
709 Schuchmann, S., Sengupta, K., Simon, M., Sipilä, M., Tauber, C., Tomé, A., Tröstl, J., Väisänen, O., Vogel,
710 A. L., Volkamer, R., Wagner, A. C., Wang, M., Weitz, L., Wimmer, D., Ye, P., Ylisirniö, A., Zha, Q., Carslaw,
711 K. S., Curtius, J., Donahue, N. M., Flagan, R. C., Hansel, A., Riipinen, I., Virtanen, A., Winkler, P. M.,
712 Baltensperger, U., Kulmala, M., and Worsnop, D. R.: Multicomponent new particle formation from
713 sulfuric acid, ammonia, and biogenic vapors, *Science Advances*, 4, eaau5363,
714 doi:10.1126/sciadv.aau5363, 2018.
- 715 Leng, C., Kish, J. D., Roberts, J. E., Dwebi, I., and Liu, Y.: Temperature-Dependent Henry's Law Constants
716 of Atmospheric Amines, *The Journal of Physical Chemistry A*, 119, 8884-8891,
717 10.1021/acs.jpca.5b05174, 2015.
- 718 Li, X., Rohrer, F., Hofzumahaus, A., Brauers, T., Häsel, R., Bohn, B., Broch, S., Fuchs, H., Gomm, S.,
719 Holland, F., Jäger, J., Kaiser, J., Keutsch, F. N., Lohse, I., Lu, K., Tillmann, R., Wegener, R., Wolfe, G. M.,
720 Mentel, T. F., Kiendler-Scharr, A., and Wahner, A.: Missing Gas-Phase Source of HONO Inferred from
721 Zeppelin Measurements in the Troposphere, *Science*, 344, 292-296, doi:10.1126/science.1248999,
722 2014.
- 723 Manninen, H. E., Nieminen, T., Asmi, E., Gagné, S., Häkkinen, S., Lehtipalo, K., Aalto, P., Vana, M.,
724 Mirme, A., Mirme, S., Hörrak, U., Plass-Dülmer, C., Stange, G., Kiss, G., Hoffer, A., Törö, N., Moerman,
725 M., Henzing, B., de Leeuw, G., Brinkenberg, M., Kouvarakis, G. N., Bougiatioti, A., Mihalopoulos, N.,
726 O'Dowd, C., Ceburnis, D., Arneth, A., Svenningsson, B., Swietlicki, E., Tarozzi, L., Decesari, S., Facchini,
727 M. C., Birmili, W., Sonntag, A., Wiedensohler, A., Boulon, J., Sellegri, K., Laj, P., Gysel, M., Bukowiecki,
728 N., Weingartner, E., Wehrle, G., Laaksonen, A., Hamed, A., Joutsensaari, J., Petäjä, T., Kerminen, V. M.,
729 and Kulmala, M.: EUCAARI ion spectrometer measurements at 12 European sites – analysis of new
730 particle formation events, *Atmos. Chem. Phys.*, 10, 7907-7927, 10.5194/acp-10-7907-2010, 2010.
- 731 Mohr, C., Lopez-Hilfiker, F. D., Zotter, P., Prevot, A. S., Xu, L., Ng, N. L., Herndon, S. C., Williams, L. R.,
732 Franklin, J. P., Zahniser, M. S., Worsnop, D. R., Knighton, W. B., Aiken, A. C., Gorkowski, K. J., Dubey,
733 M. K., Allan, J. D., and Thornton, J. A.: Contribution of nitrated phenols to wood burning brown carbon
734 light absorption in Detling, United Kingdom during winter time, *Environ Sci Technol*, 47, 6316-6324,
735 10.1021/es400683v, 2013.
- 736 Nie, W., Yan, C., Huang, D. D., Wang, Z., Liu, Y., Qiao, X., Guo, Y., Tian, L., Zheng, P., Xu, Z., Li, Y., Xu, Z.,
737 Qi, X., Sun, P., Wang, J., Zheng, F., Li, X., Yin, R., Dallenbach, K. R., Bianchi, F., Petäjä, T., Zhang, Y.,
738 Wang, M., Schervish, M., Wang, S., Qiao, L., Wang, Q., Zhou, M., Wang, H., Yu, C., Guo, H., Ye,
739 P., Lee, S., Li, Y. J., Liu, Y., Chi, X., Kerminen, V.-M., Ehn, M., Donahue, N. M., Wang, T., Huang, C.,
740 Kulmala, M., Worsnop, D., Jiang, J., and Ding, A.: Secondary organic aerosol formed by condensing
741 anthropogenic vapours over China's megacities, *Nature Geoscience*, 15, 255-261, 10.1038/s41561-
742 022-00922-5, 2022.
- 743 Paasonen, P., Nieminen, T., Asmi, E., Manninen, H. E., Petäjä, T., Plass-Dülmer, C., Flentje, H., Birmili,
744 W., Wiedensohler, A., Hörrak, U., Metzger, A., Hamed, A., Laaksonen, A., Facchini, M. C., Kerminen, V.
745 M., and Kulmala, M.: On the roles of sulphuric acid and low-volatility organic vapours in the initial
746 steps of atmospheric new particle formation, *Atmospheric Chemistry and Physics*, 10, 11223-11242,
747 10.5194/acp-10-11223-2010, 2010.
- 748 Paglione, M., Decesari, S., Rinaldi, M., Tarozzi, L., Manarini, F., Gilardoni, S., Facchini, M. C., Fuzzi, S.,
749 Bacco, D., Trentini, A., Pandis, S. N., and Nenes, A.: Historical Changes in Seasonal Aerosol Acidity in



750 the Po Valley (Italy) as Inferred from Fog Water and Aerosol Measurements, *Environ Sci Technol*, 55,
751 7307-7315, 10.1021/acs.est.1c00651, 2021.

752 Paglione, M., Saarikoski, S., Carbone, S., Hillamo, R., Facchini, M. C., Finessi, E., Giulianelli, L., Carbone,
753 C., Fuzzi, S., Moretti, F., Tagliavini, E., Swietlicki, E., Eriksson Stenström, K., Prévôt, A. S. H., Massoli, P.,
754 Canaragatna, M., Worsnop, D., and Decesari, S.: Primary and secondary biomass burning aerosols
755 determined by proton nuclear magnetic resonance (^1H -NMR) spectroscopy
756 during the 2008 EUCAARI campaign in the Po Valley (Italy), *Atmospheric Chemistry and Physics*, 14,
757 5089-5110, 10.5194/acp-14-5089-2014, 2014.

758 Paglione, M., Gilardoni, S., Rinaldi, M., Decesari, S., Zanca, N., Sandrini, S., Giulianelli, L., Bacco, D.,
759 Ferrari, S., Poluzzi, V., Scotto, F., Trentini, A., Poulain, L., Herrmann, H., Wiedensohler, A., Canonaco,
760 F., Prévôt, A. S. H., Massoli, P., Carbone, C., Facchini, M. C., and Fuzzi, S.: The impact of biomass burning
761 and aqueous-phase processing on air quality: a multi-year source apportionment study in the Po Valley,
762 Italy, *Atmospheric Chemistry and Physics*, 20, 1233-1254, 10.5194/acp-20-1233-2020, 2020.

763 Passananti, M., Zapadinsky, E., Zanca, T., Kangasluoma, J., Myllys, N., Rissanen, M. P., Kurten, T., Ehn,
764 M., Attoui, M., and Vehkamäki, H.: How well can we predict cluster fragmentation inside a mass
765 spectrometer?, *Chem Commun (Camb)*, 55, 5946-5949, 10.1039/c9cc02896j, 2019.

766 Rose, C., Sellegri, K., Velarde, F., Moreno, I., Ramonet, M., Weinhold, K., Krejci, R., Ginot, P., Andrade,
767 M., Wiedensohler, A., and Laj, P.: Frequent nucleation events at the high altitude station of Chacaltaya
768 (5240 m a.s.l.), Bolivia, *Atmospheric Environment*, 102, 18-29, 10.1016/j.atmosenv.2014.11.015, 2015.

769 Saarikoski, S., Carbone, S., Decesari, S., Giulianelli, L., Angelini, F., Canaragatna, M., Ng, N. L., Trimborn,
770 A., Facchini, M. C., Fuzzi, S., Hillamo, R., and Worsnop, D.: Chemical characterization of springtime
771 submicrometer aerosol in Po Valley, Italy, *Atmospheric Chemistry and Physics*, 12, 8401-8421,
772 10.5194/acp-12-8401-2012, 2012.

773 Schobesberger, S., Junninen, H., Bianchi, F., Lonn, G., Ehn, M., Lehtipalo, K., Dommen, J., Ehrhart, S.,
774 Ortega, I. K., Franchin, A., Nieminen, T., Riccobono, F., Hutterli, M., Duplissy, J., Almeida, J., Amorim,
775 A., Breitenlechner, M., Downard, A. J., Dunne, E. M., Flagan, R. C., Kajos, M., Keskinen, H., Kirkby, J.,
776 Kupc, A., Kurten, A., Kurten, T., Laaksonen, A., Mathot, S., Onnela, A., Praplan, A. P., Rondo, L., Santos,
777 F. D., Schallhart, S., Schnitzhofer, R., Sipilä, M., Tome, A., Tsagkogeorgas, G., Vehkamäki, H., Wimmer,
778 D., Baltensperger, U., Carslaw, K. S., Curtius, J., Hansel, A., Petaja, T., Kulmala, M., Donahue, N. M., and
779 Worsnop, D. R.: Molecular understanding of atmospheric particle formation from sulfuric acid and
780 large oxidized organic molecules, *Proc Natl Acad Sci U S A*, 110, 17223-17228,
781 10.1073/pnas.1306973110, 2013.

782 Schraufnagel, D. E.: The health effects of ultrafine particles, *Exp Mol Med*, 52, 311-317,
783 10.1038/s12276-020-0403-3, 2020.

784 Sebastian, M., Kompalli, S. K., Kumar, V. A., Jose, S., Babu, S. S., Pandithurai, G., Singh, S., Hooda, R. K.,
785 Soni, V. K., Pierce, J. R., Vakkari, V., Asmi, E., Westervelt, D. M., Hyvärinen, A.-P., and Kanawade, V. P.:
786 Observations of particle number size distributions and new particle formation in six Indian locations,
787 *Atmospheric Chemistry and Physics*, 22, 4491-4508, 10.5194/acp-22-4491-2022, 2022.

788 Shen, J., Bigi, A., Marinoni, A., Lampilahti, J., Kontkanen, J., Ciarelli, G., Putaud, J. P., Nieminen, T.,
789 Kulmala, M., Lehtipalo, K., and Bianchi, F.: Emerging Investigator Series: COVID-19 lockdown effects
790 on aerosol particle size distributions in northern Italy, *Environ Sci Atmos*, 1, 214-227,
791 10.1039/d1ea00016k, 2021.

792 Simon, M., Dada, L., Heinritzi, M., Scholz, W., Stolzenburg, D., Fischer, L., Wagner, A. C., Kürten, A.,
793 Rörup, B., He, X.-C., Almeida, J., Baalbaki, R., Baccarini, A., Bauer, P. S., Beck, L., Bergen, A., Bianchi, F.,
794 Bräkling, S., Brilke, S., Caudillo, L., Chen, D., Chu, B., Dias, A., Draper, D. C., Duplissy, J., El-Haddad, I.,
795 Finkenzeller, H., Frege, C., Gonzalez-Carracedo, L., Gordon, H., Granzin, M., Hakala, J., Hofbauer, V.,
796 Hoyle, C. R., Kim, C., Kong, W., Lamkaddam, H., Lee, C. P., Lehtipalo, K., Leiminger, M., Mai, H.,
797 Manninen, H. E., Marie, G., Marten, R., Mentler, B., Molteni, U., Nichman, L., Nie, W., Ojdanic, A.,
798 Onnela, A., Partoll, E., Petäjä, T., Pfeifer, J., Philippov, M., Quéléver, L. L. J., Ranjithkumar, A., Rissanen,
799 M. P., Schallhart, S., Schobesberger, S., Schuchmann, S., Shen, J., Sipilä, M., Steiner, G., Stozhkov, Y.,
800 Tauber, C., Tham, Y. J., Tomé, A. R., Vazquez-Pufleau, M., Vogel, A. L., Wagner, R., Wang, M., Wang, D.



801 S., Wang, Y., Weber, S. K., Wu, Y., Xiao, M., Yan, C., Ye, P., Ye, Q., Zauner-Wieczorek, M., Zhou, X.,
802 Baltensperger, U., Dommen, J., Flagan, R. C., Hansel, A., Kulmala, M., Volkamer, R., Winkler, P. M.,
803 Worsnop, D. R., Donahue, N. M., Kirkby, J., and Curtius, J.: Molecular understanding of new-particle
804 formation from α -pinene between -50 and $+25$ °C, *Atmospheric Chemistry and*
805 *Physics*, 20, 9183-9207, 10.5194/acp-20-9183-2020, 2020.

806 Sipilä, M., Sarnela, N., Jokinen, T., Henschel, H., Junninen, H., Kontkanen, J., Richters, S., Kangasluoma,
807 J., Franchin, A., Perakyla, O., Rissanen, M. P., Ehn, M., Vehkamäki, H., Kurten, T., Berndt, T., Petaja, T.,
808 Worsnop, D., Ceburnis, D., Kerminen, V. M., Kulmala, M., and O'Dowd, C.: Molecular-scale evidence
809 of aerosol particle formation via sequential addition of HIO₃, *Nature*, 537, 532-534,
810 10.1038/nature19314, 2016.

811 Stolzenburg, D., Fischer, L., Vogel, A. L., Heinritzi, M., Schervish, M., Simon, M., Wagner, A. C., Dada,
812 L., Ahonen, L. R., Amorim, A., Baccarini, A., Bauer, P. S., Baumgartner, B., Bergen, A., Bianchi, F.,
813 Breitenlechner, M., Brilke, S., Buenrostro Mazon, S., Chen, D., Dias, A., Draper, D. C., Duplissy, J., El
814 Haddad, I., Finkenzeller, H., Frege, C., Fuchs, C., Garmash, O., Gordon, H., He, X., Helm, J., Hofbauer,
815 V., Hoyle, C. R., Kim, C., Kirkby, J., Kontkanen, J., Kurten, A., Lampilahti, J., Lawler, M., Lehtipalo, K.,
816 Leiminger, M., Mai, H., Mathot, S., Mentler, B., Molteni, U., Nie, W., Nieminen, T., Nowak, J. B., Ojdanic,
817 A., Onnela, A., Passananti, M., Petaja, T., Quelevar, L. L. J., Rissanen, M. P., Sarnela, N., Schallhart, S.,
818 Tauber, C., Tome, A., Wagner, R., Wang, M., Weitz, L., Wimmer, D., Xiao, M., Yan, C., Ye, P., Zha, Q.,
819 Baltensperger, U., Curtius, J., Dommen, J., Flagan, R. C., Kulmala, M., Smith, J. N., Worsnop, D. R.,
820 Hansel, A., Donahue, N. M., and Winkler, P. M.: Rapid growth of organic aerosol nanoparticles over a
821 wide tropospheric temperature range, *Proc Natl Acad Sci U S A*, 115, 9122-9127,
822 10.1073/pnas.1807604115, 2018.

823 Stolzenburg, D., Simon, M., Ranjithkumar, A., Kürten, A., Lehtipalo, K., Gordon, H., Ehrhart, S.,
824 Finkenzeller, H., Pichelstorfer, L., Nieminen, T., He, X.-C., Brilke, S., Xiao, M., Amorim, A., Baalbaki, R.,
825 Baccarini, A., Beck, L., Bräkling, S., Caudillo Murillo, L., Chen, D., Chu, B., Dada, L., Dias, A., Dommen,
826 J., Duplissy, J., El Haddad, I., Fischer, L., Gonzalez Carracedo, L., Heinritzi, M., Kim, C., Koenig, T. K.,
827 Kong, W., Lamkaddam, H., Lee, C. P., Leiminger, M., Li, Z., Makhmutov, V., Manninen, H. E., Marie, G.,
828 Marten, R., Müller, T., Nie, W., Partoll, E., Petäjä, T., Pfeifer, J., Philippov, M., Rissanen, M. P., Rörup,
829 B., Schobesberger, S., Schuchmann, S., Shen, J., Sipilä, M., Steiner, G., Stozhkov, Y., Tauber, C., Tham,
830 Y. J., Tomé, A., Vazquez-Pufleau, M., Wagner, A. C., Wang, M., Wang, Y., Weber, S. K., Wimmer, D.,
831 Wlasits, P. J., Wu, Y., Ye, Q., Zauner-Wieczorek, M., Baltensperger, U., Carslaw, K. S., Curtius, J.,
832 Donahue, N. M., Flagan, R. C., Hansel, A., Kulmala, M., Lelieveld, J., Volkamer, R., Kirkby, J., and Winkler,
833 P. M.: Enhanced growth rate of atmospheric particles from sulfuric acid, *Atmospheric Chemistry and*
834 *Physics*, 20, 7359-7372, 10.5194/acp-20-7359-2020, 2020.

835 Ude, S. and de la Mora, J. F.: Molecular monodisperse mobility and mass standards from electrosprays
836 of tetra-alkyl ammonium halides, *Journal of Aerosol Science*, 36, 1224-1237,
837 <https://doi.org/10.1016/j.jaerosci.2005.02.009>, 2005.

838 Vana, M., Komsaare, K., Hörrak, U., Mirme, S., Nieminen, T., Kontkanen, J., Manninen, H. E., Petäjä, T.,
839 Noe, S. M., and Kulmala, M.: Characteristics of new-particle formation at three SMEAR stations, *Boreal*
840 *Environment Research*, 2016.

841 Vanhanen, J., Mikkilä, J., Lehtipalo, K., Sipilä, M., Manninen, H. E., Siivola, E., Petäjä, T., and Kulmala,
842 M.: Particle Size Magnifier for Nano-CN Detection, *Aerosol Science and Technology*, 45, 533-542,
843 10.1080/02786826.2010.547889, 2011.

844 Xiao, M., Hoyle, C. R., Dada, L., Stolzenburg, D., Kürten, A., Wang, M., Lamkaddam, H., Garmash, O.,
845 Mentler, B., Molteni, U., Baccarini, A., Simon, M., He, X.-C., Lehtipalo, K., Ahonen, L. R., Baalbaki, R.,
846 Bauer, P. S., Beck, L., Bell, D., Bianchi, F., Brilke, S., Chen, D., Chiu, R., Dias, A., Duplissy, J., Finkenzeller,
847 H., Gordon, H., Hofbauer, V., Kim, C., Koenig, T. K., Lampilahti, J., Lee, C. P., Li, Z., Mai, H., Makhmutov,
848 V., Manninen, H. E., Marten, R., Mathot, S., Mauldin, R. L., Nie, W., Onnela, A., Partoll, E., Petäjä, T.,
849 Pfeifer, J., Pospisilova, V., Quéléver, L. L. J., Rissanen, M., Schobesberger, S., Schuchmann, S., Stozhkov,
850 Y., Tauber, C., Tham, Y. J., Tomé, A., Vazquez-Pufleau, M., Wagner, A. C., Wagner, R., Wang, Y., Weitz,
851 L., Wimmer, D., Wu, Y., Yan, C., Ye, P., Ye, Q., Zha, Q., Zhou, X., Amorim, A., Carslaw, K., Curtius, J.,



852 Hansel, A., Volkamer, R., Winkler, P. M., Flagan, R. C., Kulmala, M., Worsnop, D. R., Kirkby, J., Donahue,
853 N. M., Baltensperger, U., El Haddad, I., and Dommen, J.: The driving factors of new particle formation
854 and growth in the polluted boundary layer, *Atmospheric Chemistry and Physics*, 21, 14275-14291,
855 10.5194/acp-21-14275-2021, 2021.

856 Yan, C., Yin, R., Lu, Y., Dada, L., Yang, D., Fu, Y., Kontkanen, J., Deng, C., Garmash, O., Ruan, J., Baalbaki,
857 R., Schervish, M., Cai, R., Bloss, M., Chan, T., Chen, T., Chen, Q., Chen, X., Chen, Y., Chu, B., Dällenbach,
858 K., Foreback, B., He, X., Heikkinen, L., Jokinen, T., Junninen, H., Kangasluoma, J., Kokkonen, T., Kurppa,
859 M., Lehtipalo, K., Li, H., Li, H., Li, X., Liu, Y., Ma, Q., Paasonen, P., Rantala, P., Pileci, R. E., Rusanen, A.,
860 Sarnela, N., Simonen, P., Wang, S., Wang, W., Wang, Y., Xue, M., Yang, G., Yao, L., Zhou, Y., Kujansuu,
861 J., Petäjä, T., Nie, W., Ma, Y., Ge, M., He, H., Donahue, N. M., Worsnop, D. R., Veli-Matti, K., Wang, L.,
862 Liu, Y., Zheng, J., Kulmala, M., Jiang, J., and Bianchi, F.: The Synergistic Role of Sulfuric Acid, Bases, and
863 Oxidized Organics Governing New-Particle Formation in Beijing, *Geophysical Research Letters*, 48,
864 10.1029/2020gl091944, 2021.

865 Yan, C., Nie, W., Vogel, A. L., Dada, L., Lehtipalo, K., Stolzenburg, D., Wagner, R., Rissanen, M. P., Xiao,
866 M., Ahonen, L., Fischer, L., Rose, C., Bianchi, F., Gordon, H., Simon, M., Heinritzi, M., Garmash, O.,
867 Roldin, P., Dias, A., Ye, P., Hofbauer, V., Amorim, A., Bauer, P. S., Bergen, A., Bernhammer, A.-K.,
868 Breitenlechner, M., Brilke, S., Buchholz, A., Mazon, S. B., Canagaratna, M. R., Chen, X., Ding, A.,
869 Dommen, J., Draper, D. C., Duplissy, J., Frege, C., Heyn, C., Guida, R., Hakala, J., Heikkinen, L., Hoyle, C.
870 R., Jokinen, T., Kangasluoma, J., Kirkby, J., Kontkanen, J., Kürten, A., Lawler, M. J., Mai, H., Mathot, S.,
871 Mauldin, R. L., Molteni, U., Nichman, L., Nieminen, T., Nowak, J., Ojdanic, A., Onnela, A., Pajunaja, A.,
872 Petäjä, T., Piel, F., Quéléver, L. L. J., Sarnela, N., Schallhart, S., Sengupta, K., Sipilä, M., Tomé, A., Tröstl,
873 J., Väisänen, O., Wagner, A. C., Ylisirniö, A., Zha, Q., Baltensperger, U., Carslaw, K. S., Curtius, J., Flagan,
874 R. C., Hansel, A., Riipinen, I., Smith, J. N., Virtanen, A., Winkler, P. M., Donahue, N. M., Kerminen, V.-
875 M., Kulmala, M., Ehn, M., and Worsnop, D. R.: Size-dependent influence of NO_x on the
876 growth rates of organic aerosol particles, *Science Advances*, 6, eaay4945, doi:10.1126/sciadv.aay4945,
877 2020.

878 Yao, L., Wang, M.-Y., Wang, X.-K., Liu, Y.-J., Chen, H.-F., Zheng, J., Nie, W., Ding, A.-J., Geng, F.-H., Wang,
879 D.-F., Chen, J.-M., Worsnop, D. R., and Wang, L.: Detection of atmospheric gaseous amines and amides
880 by a high-resolution time-of-flight chemical ionization mass spectrometer with protonated ethanol
881 reagent ions, *Atmospheric Chemistry and Physics*, 16, 14527-14543, 10.5194/acp-16-14527-2016,
882 2016.

883 Yao, L., Garmash, O., Bianchi, F., Zheng, J., Yan, C., Kontkanen, J., Junninen, H., Mazon, S. B., Ehn, M.,
884 Paasonen, P., Sipilä, M., Wang, M. Y., Wang, X. K., Xiao, S., Chen, H. F., Lu, Y. Q., Zhang, B. W., Wang,
885 D. F., Fu, Q. Y., Geng, F. H., Li, L., Wang, H. L., Qiao, L. P., Yang, X., Chen, J. M., Kerminen, V. M., Petaja,
886 T., Worsnop, D. R., Kulmala, M., and Wang, L.: Atmospheric new particle formation from sulfuric acid
887 and amines in a Chinese megacity, *Science*, 361, 278-+, 10.1126/science.aao4839, 2018.

888 Yu, H., Zhou, L., Dai, L., Shen, W., Dai, W., Zheng, J., Ma, Y., and Chen, M.: Nucleation and growth of
889 sub-3 nm particles in the polluted urban atmosphere of a megacity in China, *Atmospheric Chemistry
890 and Physics*, 16, 2641-2657, 10.5194/acp-16-2641-2016, 2016.

891 Zha, Q., Huang, W., Aliaga, D., Peräkylä, O., Heikkinen, L., Koenig, A. M., Wu, C., Enroth, J., Gramlich,
892 Y., Cai, J., Carbone, S., Hansel, A., Petäjä, T., Kulmala, M., Worsnop, D., Sinclair, V., Krejci, R., Andrade,
893 M., Mohr, C., and Bianchi, F.: Measurement report: Molecular-level investigation of atmospheric
894 cluster ions at the tropical high-altitude research station Chacaltaya (5240 m a.s.l.) in the Bolivian
895 Andes, *Atmospheric Chemistry and Physics*, 23, 4559-4576, 10.5194/acp-23-4559-2023, 2023.

896 Zha, Q., Yan, C., Junninen, H., Riva, M., Sarnela, N., Aalto, J., Quéléver, L., Schallhart, S., Dada, L.,
897 Heikkinen, L., Peräkylä, O., Zou, J., Rose, C., Wang, Y., Mammarella, I., Katul, G., Vesala, T., Worsnop,
898 D. R., Kulmala, M., Petäjä, T., Bianchi, F., and Ehn, M.: Vertical characterization of highly oxygenated
899 molecules (HOMs) below and above a boreal forest canopy, *Atmospheric Chemistry and Physics*, 18,
900 17437-17450, 10.5194/acp-18-17437-2018, 2018.

901 Zheng, Y., Chen, Q., Cheng, X., Mohr, C., Cai, J., Huang, W., Shrivastava, M., Ye, P., Fu, P., Shi, X., Ge,
902 Y., Liao, K., Miao, R., Qiu, X., Koenig, T. K., and Chen, S.: Precursors and Pathways Leading to Enhanced

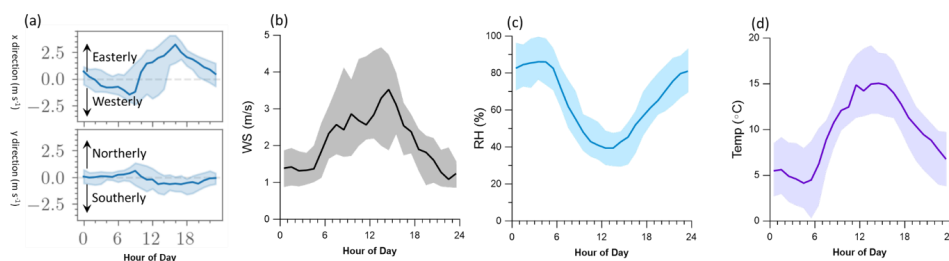


903 Secondary Organic Aerosol Formation during Severe Haze Episodes, *Environ Sci Technol*, 55, 15680-
904 15693, 10.1021/acs.est.1c04255, 2021.
905 Zhu, S., Yan, C., Zheng, J., Chen, C., Ning, H., Yang, D., Wang, M., Ma, Y., Zhan, J., Hua, C., Yin, R., Li, Y.,
906 Liu, Y., Jiang, J., Yao, L., Wang, L., Kulmala, M., and Worsnop, D. R.: Observation and Source
907 Apportionment of Atmospheric Alkaline Gases in Urban Beijing, *Environ Sci Technol*, 56, 17545-17555,
908 10.1021/acs.est.2c03584, 2022.

909



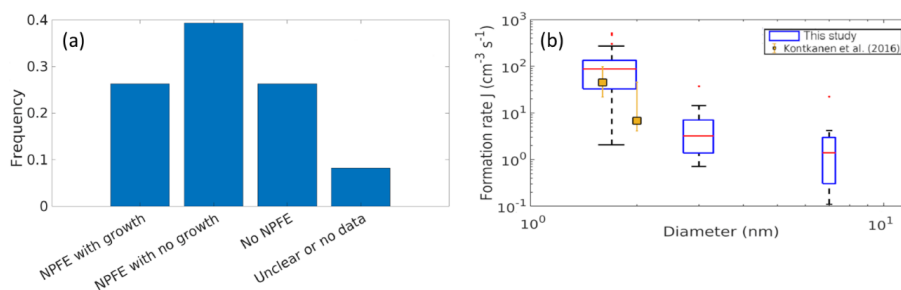
910



911

912 **Figure 1.** The diurnal variations of (a) average wind vectors, (b) wind speed, (c) relative humidity (RH), and (d)
 913 temperature.

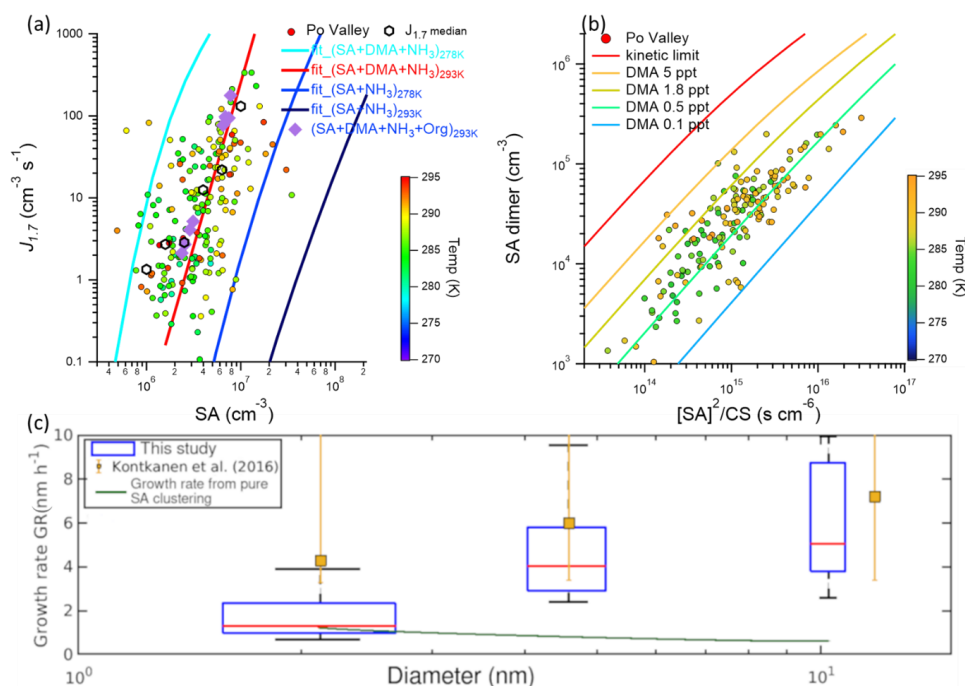
914



915

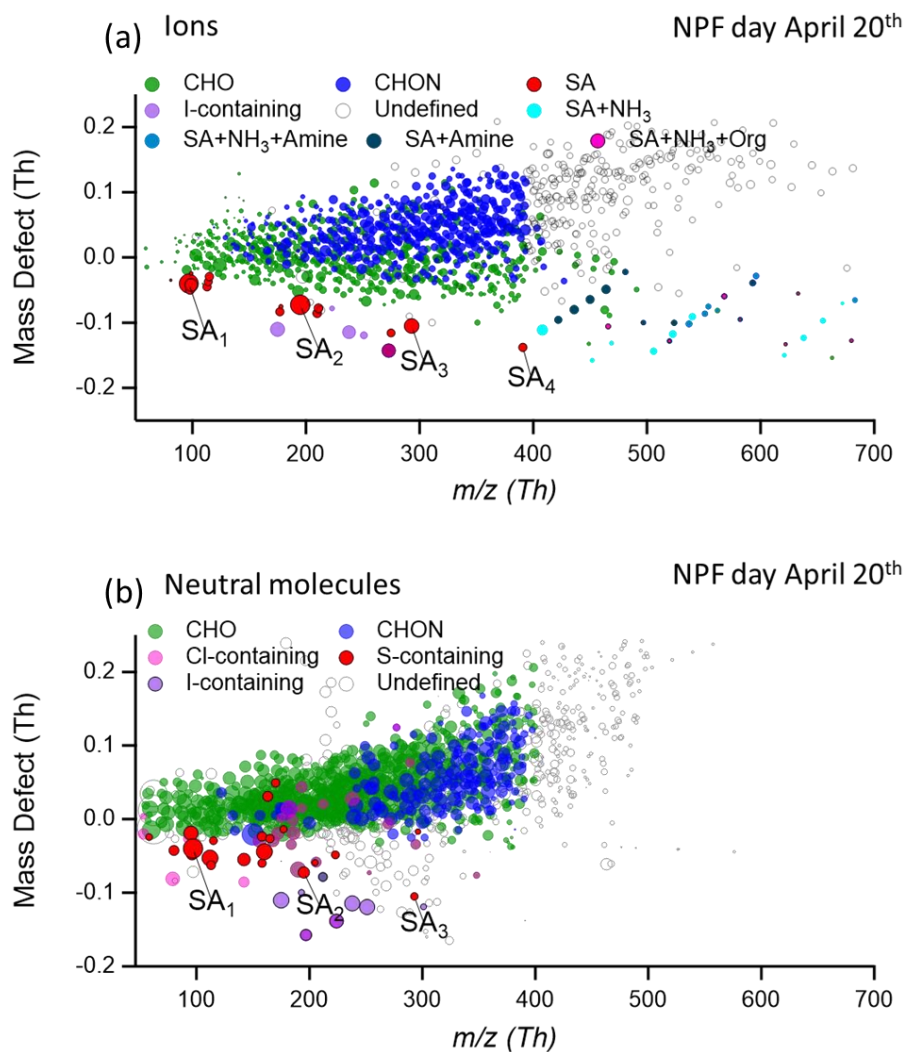
916 **Figure 2.** (a) The frequency of NPF events with and without growth, of days without NPF, and days with unclear
 917 classification or no data during this study, (b) calculated formation rates at 1.7 nm, 3 nm and 7 nm from this
 918 study and values reported by Kontkanen et al. 2016 (yellow squares). The red lines are the median values of the
 919 maximum formation rates measured during an NPF event, the blue boxes show the values between 25th and 75th
 920 percentiles and the black whiskers mark the 5th and 95th percentiles. Red dots are outliers, and the width of the
 921 box is proportional to the square root of the number of the J values.

922



923

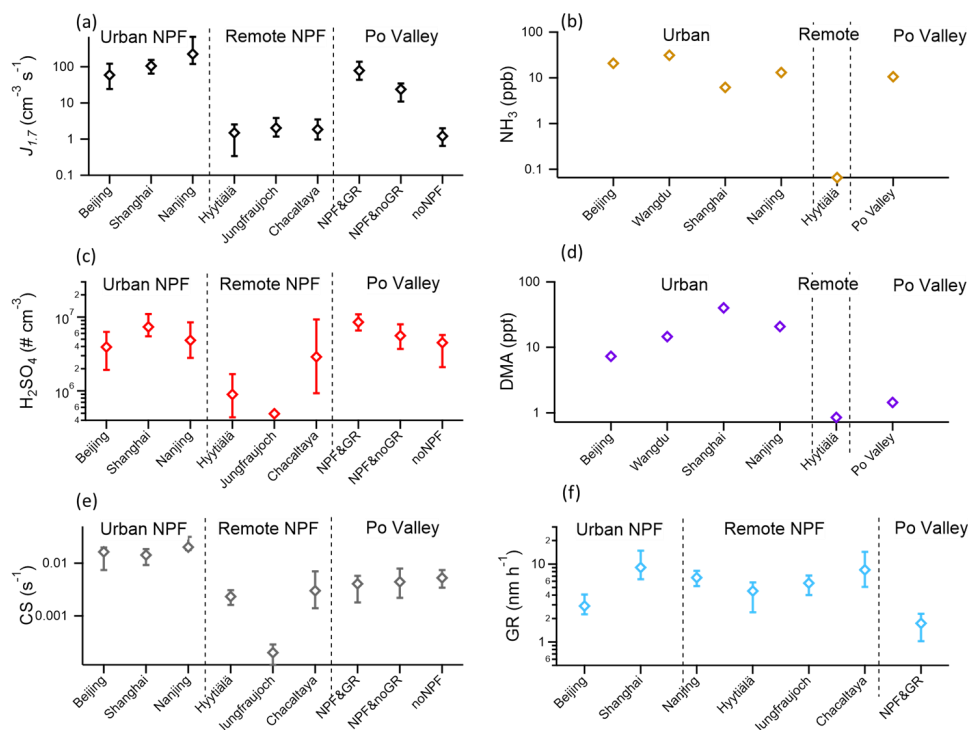
924 **Figure 3.** (a) The formation rate of 1.7 nm particles ($J_{1,7}$) versus SA concentrations in during springtime in the Po
 925 Valley (shown as circles) and experimental results from CLOUD chamber experiments (shown as solid diamonds).
 926 The solid lines are from fitted results of CLOUD chamber experiments and the black hexagon represented the
 927 mean values under different SA levels, (b) the relationship between sulfuric acid dimer concentration (SA dimer),
 928 the square of monomer concentrations (SA)², and the CS. The lines are from the kinetic model simulations under
 929 different DMA levels and the dots are from the measurement. In (a) and (b), the results from the field
 930 measurements are from the daytime (10:00 – 14:00 LT) and color-coded by the temperature at the site. The $J_{1,7}$
 931 and corresponding SA concentrations of CLOUD chamber results are from previous literature (Xiao et al., 2021).
 932 (c) Calculated growth rates for 1.5 – 3 nm, 3 – 7 nm, and 7 – 15 nm from this study and values reported by
 933 Kontkanen et al. (2016, yellow squares). The red horizontal lines are the median values, the blue boxes show the
 934 values between 25th and 75th percentiles and the black whiskers mark the 5th and 95th percentiles. The green solid
 935 line represents predicted growth rates from pure sulfuric acid without organics condensation (Stolzenburg et al.,
 936 2020). The width of the box is proportional to the square root of the number of the GR values.



937

938 **Figure 4.** Mass defect plots, which represent the difference between compounds' exact mass and nominal mass,
939 for (a) ion clusters and (b) neutral clusters during the NPF period (10:00 – 14:00 LT) of April 20. The size of the
940 dots is proportional to the logarithm of the signal intensity of each cluster.

941



942

943 **Figure 5.** Parameters and gaseous precursors of NPF in the Po Valley and other environments. (a) formation rate
 944 of sub-2 nm particles, (b) the atmospheric NH_3 concentrations, (c) SA concentrations, (d) DMA concentrations,
 945 (e) CS levels, and (f) growth rate in different environments. The diamond dots represent the median values, and
 946 the error bars represent the 25th and 75th percentiles. For the Po Valley data, the formation rates, growth rates, SA
 947 concentrations and CS data were selected for 10:00 – 14:00 LT. The formation rates, growth rates, SA
 948 concentrations and CS during NPF in Beijing, Shanghai, Hyvitiälä, Jungfraujoch and Chacaltaya are from Deng
 949 et al. (2020). The GR calculation range varies for different sites. Beijing (GR_{7-15} , (Deng et al., 2020)), Shanghai
 950 (GR_{7-25} , (Yao et al., 2018)), Nanjing (GR_{3-20} , (Yu et al., 2016)), Hyvitiälä (GR_{3-20} , (Vana et al., 2016)),
 951 Jungfraujoch (GR_{7-20} , (Boulon et al., 2010)), Chacaltaya (GR_{7-20} , (Rose et al., 2015)), and Po Valley (GR_{7-15} , this
 952 study) are used for comparison. The NH_3 and DMA concentrations are from literature, which is listed in the Table
 953 S1. Half of the limit of detection (LOD) of DMA concentrations in Hyvitiälä was applied in panel d. DMA
 954 concentrations in Po Valley was not presented since it is not quantified in this study.